Department of Construction Sciences
Solid Mechanics

ISRN LUTFD2/TFHF-19/5234-SE(1-71)

Material characterization of 316L

Master's Dissertation by

Pardis Adibi

and

Rita Iteka

Supervisors:

Johan Jeppsson, FS Dynamics

Anders Ericsson, Div. of Solid Mechanics

Examiner:

Prof. Matti Ristinmaa, Div. of Solid Mechanics

Printed by Media-Tryck AB, Lund, Sweden

For information, address:

Division of Solid Mechanics, Lund University, Box 118, SE-221 00 Lund, Sweden

Webpage: www.solid.lth.se

Acknowledgements

We would like to start off by thanking everyone who have been involved in the project. We are thankful for FS Dynamics and Tetra Pak for giving us the opportunity to do our master thesis. Many thanks to Fredrik Liljedahl together with our colleagues for creating a nice environment to work in.

Special thanks to our supervisors Johan Jeppsson and Anders Ericsson. Johan gave us constant guidance in all parts of the study, from modeling, simulation and interpretation of results. With his expertise and patience we were able to get many valuable discussions.

Anders gave us the academic support we needed to further understand the theory behind material characterization. The continuous feedback from him during the project was also of great value. We are thankful for Matti Ristinmaa for keeping us on the right track during the early stages. And for all the knowledge we were able to obtain from his book.

We are greatful for Eskil Andreasson at Tetra Pak for being active in the discussions concerning our work. He showed great interest in the study and gave many valuable tips regarding both physical and virtual experiments.

We would like to thank the people at Department of Mechanical Engineering for their help and guidance with the experiments, especially Dmytro Orlov and Jonas Engqvist. We are also thankful for Fredrik Ottenklev who could exchange ideas with us regarding the material and tensile testing.

Abstract

At Tetra Pak®, general knowledge of food and beverage processing is of great importance. This in turn, depends on the equipment used for the particular process. One of these equipment consists of deformed tubes made of stainless steel 316L. The aim of the present work is to get an understanding of the material 316L. To achieve this, physical tensile tests are performed to study the material behaviour under quasistatic and dynamic loading conditions. Virtual tensile tests are created where the material behaviour is described with existing material models in Abaqus/-Explicit. The proposed material models are Bilinear, Multilinear and Johnson-Cook isotropic hardening models. A material model is today used to describe the material behaviour and is compared with the proposed material models.

For quasistatic cases, the findings in virtual tensile tests compared to experimental data are: the multilinear and the Johnson-Cook models give a good prediction of plastic behaviour, whereas the bilinear model gives a rough estimation of plastic deformation. In addition, use of the proposed material models result in a stiffer response of the material in comparison with the currently used material model. For dynamic cases, effects of strain-rates on material properties are investigated using isotropic hardening combined with rate-dependent models such as Cowper-Symonds and Johnson-Cook in Abaqus/Explicit. It is found that there are different approaches to determine the parameters in these material models, making it hard to verify the accuracy. In spite of the fact, the results from the study indicate that the material is rate-dependent. Therefore, a rate-dependent material model is necessary to capture the material behaviour.

Sammanfattning

På Tetra Pak utgör processutrustningar en viktig del av den slutliga livsmedelsprodukten, därför är ökad kunskap av utrustningarna av stor betydelse. En av dessa utrustningar består av deformerade rör av materialtypen rostfritt stål 316L. Målet med arbetet är att få ökad förståelse av materialet vid belastning. För att uppnå målet, har både fysiska och virtuella dragprov utformats i syfte att studera materialbeteendet under kvasistatiska och dynamiska belastningsfall. De simulerade dragproven är skapade med materialmodeller som är tillgängliga i Abaqus/Explicit. Tre materialmodeller med isotropiskt hårdnande har föreslagits, nämligen: bilinjär, multilinjär och Johnson-Cook. För nuvarande beskrivs materialbeteendet med en annan materialmodell, vilken jämförs med de ovannämnda materialmodeller.

Resultaten av kvasistatisk belastningsfall, vid jämförelse av fysiska och virtuella experiment, visar att: den multilinjära och Johnson-Cook modellen fångar upp materialbeteendet både i elastisk och plastisk område. Till skillnad från den bilinjär modellen som ger en grov anpassning till plastisk deformation. Tillsammans, visar de föreslagna materialmodeller att materialet svarar styvare än den materialmodell som används idag. Vid dynamisk belastningsfall, har töjningshastighetsberoendet studerats och beskrivits med Cowper-Symonds och Johnson-Cook i Abaqus/Explicit. Studier avslöjar att parametrar i dessa modeller tas fram på olika sätt och med olika experiment, därför är det svårt att avgöra noggranheten i resultaten. Trots det, visar resultaten att materialet har en klar beroende av töjningshastigheten. Därmed kan slutsatser dras att en materialmodell som fångar upp beroendet är nödvändig för att beskriva materialbeteendet med större noggranhet.

Contents

List of Figures

List of Tables

Nomenclature

δ_{ij}	Kronecker delta
$\dot{\beta}$	Time-independent quantity
$\dot{\lambda}$	Plastic strain multiplier
$\dot{\varepsilon}^{e}_{ij}$	Elastic strain rate tensor
$\dot{\varepsilon}^{p}_{ij}$	Plastic strain rate tensor
$\dot{\varepsilon}^{vp}_{ij}$	Viscoplastic strain rate tensor
η	Viscosity parameter
λ, μ	Lame's parameters
ν	Poisson's ratio
σ_y	Yield stress
σ_{eff}	Effective stress
σ_{ij}	Second order stress tensor
σ_{kk}	Dilatation
ε^{p}_{ij}	Plastic strain tensor
ε^{e}_{ij}	Elastic strain tensor
ε^{p}_{eff}	Effective plastic strain

ε_{ij} Second order strain tensor

ε_{kk} Dilatation

$A, B, n, C, \dot{\varepsilon}_0$ and m Johnson-Cook parameters

D, p Cowper-Symonds parameters

$d\sigma$ Stress increment

$d\varepsilon$ Strain increment

D_{ijkl} Elastic stiffness tensor

E Young's modulus

E_T Tangent modulus

H Plastic or work hardening modulus

I_1 First deviatoric stress invariant (Hydrostatic stress)

J_2 Second deviatoric stress invariant

K Hardening parameter

s_{ij} Deviatoric stress tensor

T_{melt} Melting temperature

T_{room} Room temperature

α_{ij} von Mises surface center in the deviatoric plane

κ Internal invariable

1 Introduction

1.1 Presentation of Tetra Pak and FS Dynamics

Tetra Pak is a world leading food processing and packaging solutions company. FS Dynamics is a consultant company and is the leading CAE supplier in Scandinavia who optimizes technology in industrial companies. This thesis is a collaboration between the two companies.

1.2 Background

At Tetra Pak® processing equipment, filling machines and distribution equipment is an integrated unit at the customer sites when producing package liquid foods. When developing new concept and designs, performing simulations is a natural part of the design work. It is also used to simulate the manufacturing process. To be able to do this a more accurate material model is of interest.

1.3 Purpose

The creation of more realistic and predictive simulation models is essential for the future to complement the current development and manufacturing process. A computer model is today present to create this deformation of steel tubes virtually to be used to increased understanding of the different load cases and factors involved during the manufacturing process. This virtual manufacturing replica is used to iterate, optimize and improve design loops and functionality of the deformation process.

1.4 Objective

Through experimental testing, especially tensile testing, and then establishing a virtual model of the test, the material 316L stainless steel can be characterized and thereafter analyzed to establish a representative material model.

1.5 Limitations

Different studies on 316L stainless steel have been made by many researchers, which could be found in the various articles and books. However, the results vary widely due to different factors such as heat treatment and other processes that are not always mentioned in these studies, making it difficult to compare with the material issued for this study.

Abaqus was used for analyzing the virtual test with different material models. This limits the types of models that can be applied, more advanced material models would require a so-called user-defined material model (VUMAT).

Tensile tests were performed using Instron ElectroPuls^{TM}. Performing high strain-rate tests with this machine (from $10^{-1}s^{-1}$) resulted in very noisey load curves that could not be used for analysis. After contacting several people that have experience using the machine, including Instron Service group, the misses in technical set-up that may have caused it were not found until at the end of the project.

1.6 Methods

The next chapters that are presented follow the work flow for this master thesis. Starting of is a literature study on general material behaviour of steels and metals as well as research that has been done on stainless steel 316L. Following are the proposed material models that are commonly used for this material and how they relate to theory on material behaviour. A study on how standard tensile tests are performed is also done, which is used to find standard geometry and standard testing methods for steel. The next step is a description of the methodology on the tensile testing and the results obtained from it. The results are then calibrated and interpretations of them are presented. From that, a virtual model is created in HyperMesh, and results from virtual tensile tests in Abaqus/Explicit are compared with the physical tensile tests. In reality, the comparison between physical and virtual experiments is made iteratively. Finally, the deformation process is evaluated and the findings from the study are presented.

2 Theory

In the following chapter, general theories of material behaviour are discussed and how they are applied for steels and metals. These behaviours are obtained by deforming the material. A description of the behaviour is then provided by the applied loading and is then converted to the so-called stress and strain tensor. The relationship between stresses and strains is called the *constitutive relation*. Some examples of such relations are *elasticity, plasticity* and *viscoplasticity* and they will be summarized in this chapter.

2.1 Linear elasticity

An elastic material returns completely to its original configuration after removal of the applied force. The small strain behaviour of the metals can be defined by a linear stress-strain relationship, called *Hooke's law* suggested by Hooke in 1676,

$$\sigma_{ij} = D_{ijkl}\varepsilon_{kl} \tag{2.1}$$

where σ_{ij} is the stress tensor, D the elastic stiffness tensor and ε_{ij} is the strain tensor. For an isotropic material, the response to the loading is independent on loading direction. For this type of material, the elastic stiffness tensor has only two independent material parameters, called *Lamé's* parameters, μ and λ. Since these parameters are constants, the stress-strain relationship in (2.1) is linear, defined as,

$$\sigma_{ij} = \lambda\varepsilon_{kk}\delta_{ij} + 2\mu\varepsilon_{ij} \tag{2.2}$$

These material parameters can be expressed as follows,

$$\lambda = \frac{\nu E}{(1+\nu)(1-2\nu)}, \qquad \mu = \frac{E}{2(1+v)} \tag{2.3}$$

where E is the Young's modulus and ν is the Poisson's ratio. A definition of the stress deviatoric tensor is given by,

$$s_{ij} = \sigma_{ij} - \frac{1}{3}\sigma_{kk}\delta_{ij} \tag{2.4}$$

where $\sigma_{kk}/3 = I_1$ is called the hydrostatic stress and δ_{ij} is the Kronecker delta [1]. Use of this definition together with Eq. (2.3), the constitutive relation (2.2) becomes as formulated in Eq. (2.1), where D_{ijkl} becomes the elastic isotropic stiffness tensor defined as,

$$D_{ijkl} = 2\mu\left[\frac{1}{2}(\delta_{ik}\delta_{jl} + \delta_{il}\delta_{jk}) + \frac{\nu}{1-2\nu}\delta_{ij}\delta_{kl}\right] \tag{2.5}$$

A material is anisotropic if it has different responses in different loading directions. It means that the constitutive relation takes different forms depending on the choice of Cartesian coordinate system.

2.2 Metal plasticity

On the contrary to elasticity, the plasticity describes the permanent deformation of a material due to applied load. A metal subjected to a load, deforms elastically until the stress reaches point A as illustrated in Fig. 2.1. If the load exceeds a certain value, σ_y, the material starts to deform plastically. When the applied load is removed, the material retains its new configuration, with remaining plastic strain illustrated as point B,

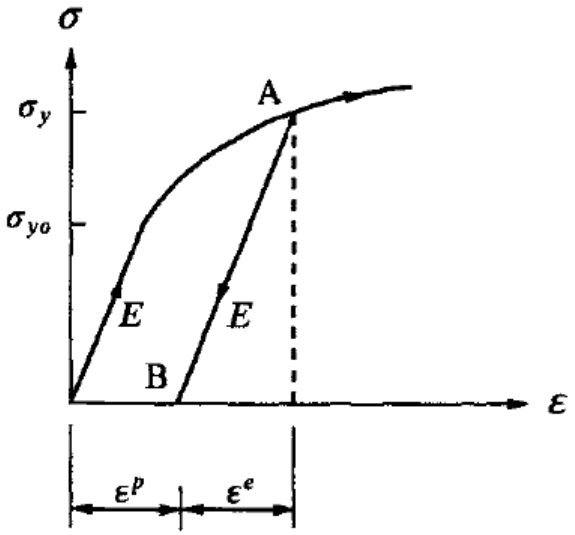

Figure 2.1: Stress-strain curve of elasto-plastic material. [1]

The total strain rate can be expressed in terms of the elastic and plastic strain rate as,

$$\dot{\varepsilon}_{ij} = \dot{\varepsilon}^e_{ij} + \dot{\varepsilon}^p_{ij} \tag{2.6}$$

The integrated form of (2.6) with respect to time is,

$$\varepsilon_{ij} = \varepsilon^e_{ij} + \varepsilon^p_{ij} \tag{2.7}$$

In order to understand the differences between the elastic and plastic response, the following relations are to be represented and formulated,

- *Yield surface*
- *Hardening rule*
- *Flow rule*

2.2.1 Yield surface

The yield surface defines when yielding occurs and separates the elastic and plastic region. The initial yield strength, σ_{y0}, is defined as the point on the stress-strain curve at which 0.2% plastic deformation occurs. For development of plasticity, the yield surface can be defined as a criterion, i.e. a function of the stress state and the hardening parameter K such as,

$$f(\sigma_{ij}, K) = 0 \tag{2.8}$$

The hardening parameter depends only on an internal variable κ, i.e. $K = K(\kappa)$. This variable describes the state of the material and can be a scalar or a higher-order tensor. An example of an internal variable is the effective plastic strain, ε^p_{eff}. The sign of the yield function defines in which region the material is located,

$$\begin{cases} f(\sigma_{ij}, K) < 0 & \text{elastic behaviour} \\ f(\sigma_{ij}, K) = 0 & \text{development of plasticity} \end{cases}$$

There are different forms of yield criteria, such as, von Mises, Hill, Tresca and Drucker-Prager. The von Mises yield criterion is often used for ductile materials, such as steels and metals, and will therefore be used in this study. This criterion for the initial yield suggests that yielding occurs when the second deviatoric stress invariant, J_2 reaches a certain value according to,

$$f = \sqrt{3J_2} - \sigma_{y0} = 0; \quad J_2 = \frac{1}{2} s_{ij} s_{ji} \tag{2.9}$$

When analyzing plastic deformation of metals and steels, yielding turns out to be independent of the hydrostatic stress $I_1 = \sigma_{kk}/3$. For this reason J_2 takes a constant value at yielding. Defining the effective stress as $\sigma_{eff} = \sqrt{3J_2}$, relation (2.9) can be rewritten as,

$$f = \sigma_{eff} - \sigma_{y0} = 0 \tag{2.10}$$

The effective stress can also be expressed in terms of the principal stresses as,

$$\sigma_{eff} = \sqrt{\frac{1}{2}\Big[(\sigma_1 - \sigma_2)^2 + (\sigma_1 - \sigma_3)^2 + (\sigma_2 - \sigma_3)^2\Big]} \tag{2.11}$$

where σ_1, σ_2 and σ_3 are the principal stresses. It appears that the von Mises yield surface represents a cylindrical surface in the Haigh-Westergard principal stress space shown in Fig. 2.2.

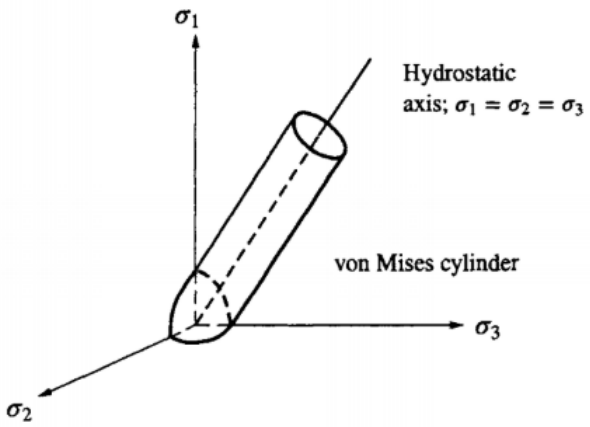

Figure 2.2: von Mises surface in the principal stress space [1].

2.2.2 Hardening rule

During inelastic straining process, hardening in the material occurs due to rearrangement of the microstructure of the material. This can be modified by complex loading paths or by aging of the material and is expressed through hardening models. In mathematical terms, hardening rule translates to how the yield surface changes with the plastic loading. The common hardening types are the *isotropic* and *kinematic hardening*. [3]

Kinematic and isotropic hardening

The simplest hardening model is called isotropic hardening. It occurs due to the expansion of the yield surface when the initial yield condition is exceeded. Isotropic hardening for an arbitrary yield function can be formulated as,

$$f(\sigma_{ij}, K) = F(\sigma_{ij}) - K = 0 \tag{2.12}$$

With the von Mises yield condition given in (2.9), this is represented as an expanding radius with κ as a scalar variable,

$$f(\sigma_{ij}, K) = \sigma_{eff} - \sigma_y(\kappa) = 0, \qquad \sigma_y(\kappa) = \sigma_{y0} + K(\kappa) \tag{2.13}$$

where σ_y is the current stress state. In the case of kinematic hardening, the translation of the yield surface is described with a tonsorial variable that defines the center. An illustrative explanation of the aforementioned hardening rules is seen in Fig. 2.3. For an arbitrary yield function, the kinematic hardening can be defined as,

$$f(\sigma_{ij}, K) = F(\sigma_{ij} - \alpha_{ij}) = 0 \tag{2.14}$$

This function for the von Mises criterion can be derived as,

$$f(\sigma_{ij}, K) = \left[\frac{3}{2}(s_{ij} - \alpha_{ij})(s_{ij} - \alpha_{ij})\right]^{1/2} - \sigma_{y0} = 0 \tag{2.15}$$

where the tensor α_{ij} defines the center of the von Mises surface in the deviatoric plane.

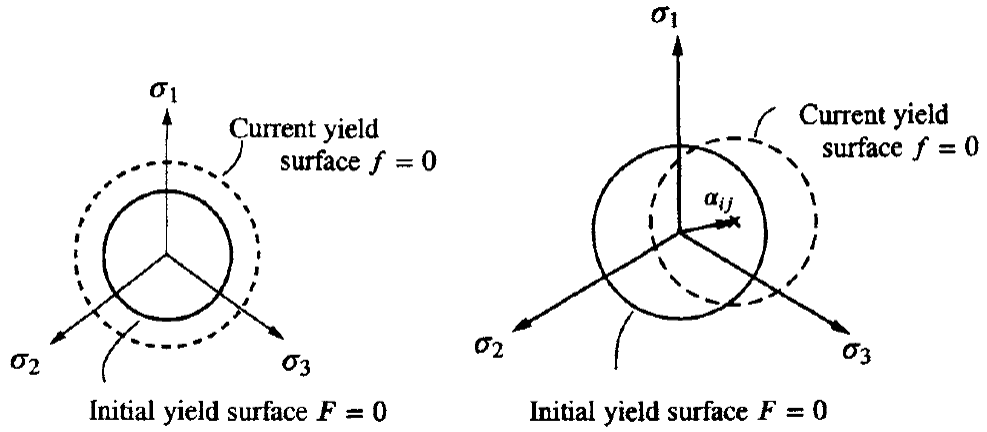

Figure 2.3: (Left) Isotropic hardening; an expansion of the initial yield surface. (Right) Kinematic hardening; a translation of the initial yield surface [1].

2.2.3 Flow rule

As mentioned, the elastic strain can be calculated using the *Hooke's law*. In order to calculate the plastic strain, a constitutive law should be derived, called *flow rule*. In other words, the flow rule is a constitutive law for $\dot{\varepsilon}^p_{ij}$. *Lévy* and *von Mises* separately suggested that the plastic strain increment and the deviatoric stresses have the same direction. This relation is called the *Lévy-von Mises equations*,

$$\dot{\varepsilon}_{ij} = \dot{\beta} s_{ij}, \qquad \dot{\beta} \geq 0 \tag{2.16}$$

where $\dot{\beta}$ is a time-independent quantity. $\dot{\beta} = 0$ indicates that no strains develop. Relation (2.16) assumes that the elastic strain is zero, which means the total strain is equal to the plastic strain. A new format of (2.16) was suggested by *Prandtl* and *Reuss* as,

$$\dot{\varepsilon}^p_{ij} = \dot{\beta} s_{ij}; \qquad \dot{\beta} \geq 0 \tag{2.17}$$

Differentiation of (2.13) with respect to the stress tensor gives,

$$\frac{\partial f}{\partial \sigma_{ij}} = \frac{3s_{ij}}{2\sqrt{3J_2}} = \frac{3}{2}\frac{s_{ij}}{\sigma_y} \tag{2.18}$$

Combination of Eq. (2.17) and Eq. (2.18) gives the flow rule,

$$\dot{\varepsilon}^p_{ij} = \dot{\lambda}\frac{\partial f}{\partial \sigma_{ij}}; \qquad \dot{\lambda} \geq 0 \tag{2.19}$$

where $\dot{\lambda} = 2\sigma_y\dot{\beta}/3$ is the incremental plastic strains. The effective plastic strain rate becomes,

$$\dot{\varepsilon}^p_{eff} = \sqrt{\frac{2}{3}\dot{\varepsilon}^p_{ij}\dot{\varepsilon}^p_{ij}} \tag{2.20}$$

which integrated with respect to time gives the effective plastic strain as,

$$\varepsilon^p_{eff} = \int_0^t \dot{\varepsilon}^p_{eff} dt \tag{2.21}$$

2.3 Viscoplasticity

Viscoplasticity has become of interest in the last decades after it was observed that some materials could not be categorized as neither viscoelastic nor as viscous. It turns out, that some viscous materials require a certain amount of stress in order to show viscous effects. Viscoplasticity describes the rate-dependent plastic behaviour of materials. Rate-dependence in this context means that the strains depend non-linearly on the rate at which the stresses are applied. This type of plasticity is usually modeled by the Perzyna overstress model. Perzyna proposed the following formulation,

$$\dot{\varepsilon}^{vp}_{ij} = \begin{cases} 0 & \text{if} \quad f(\sigma_{ij}, K) \leq 0 \\ \frac{\Phi(f(\sigma_{ij},K))}{\eta}\frac{\partial f}{\partial \sigma_{ij}} & \text{if} \quad f(\sigma_{ij}, K) > 0 \end{cases} \tag{2.22}$$

The function $\Phi(f)$ is the overstress that depends on the yield surface and $\Phi(f = 0) = 0$ is required. There are some differences between Perzyna model and time-independent plasticity. The Perzyna viscoplasticity (2.22) allows one to choose the factor $\frac{\Phi(f)}{\eta}$, whereas the plastic multiplier $\dot{\lambda}$, (see Eq. 2.19) is obtained using the consistency relation. In order for viscoplastic strains to develop, the stresses must be located outside the time-independent yield surface. However, in case of the time-independent plasticity, the stresses are not allowed to be located outside the yield surface.

2.4 Rate independent constitutive relation

The constitutive relation which describes the relation between stresses and strains, is called *material model*. This mathematical model can predict the response of materials to various loading conditions. Some of the fundamental equations that are needed to form a constitutive relation have been introduced. With this in mind, the material models that are frequently used for 316L, will now be presented and how they relate to the fundamental equations. The focus in this section will be on how they are applied for quasistatic cases.

2.4.1 Bilinear isotropic hardening model

The bilinear model is a common non-linear material model used for metals. This model can be defined with different yield criteria. For metals, von Mises is used to describe the yield surface with the isotropic hardening shown in Eq. (2.13). The internal variable κ is chosen as $\kappa = \varepsilon^p_{eff}$.

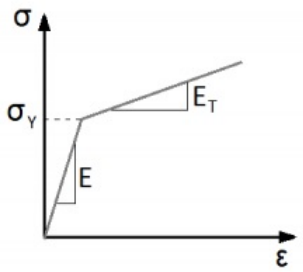

Figure 2.4: An example of a bilinear material model curve.

In this model, materials exhibit a characteristic called *linear work-hardening*. After initial yielding, stress varies linearly with plastic strain. At any point, the increment of stress is related to the increment of strain as,

$$d\sigma = E_T d\varepsilon \tag{2.23}$$

The slope of the curve at the plastic region is called *tangent modulus*, denoted as E_T. From relation (2.7), the increment of strain consists of both elastic and plastic strain after yielding becomes,

$$d\varepsilon = d\varepsilon^e + d\varepsilon^p \tag{2.24}$$

Plastic modulus H is the slope of stress vs. plastic strain as follows,

$$d\sigma = H d\varepsilon^p \tag{2.25}$$

Using (2.23), (2.24), (2.25) and Hooke's law gives,

$$\frac{1}{E_T} = \frac{1}{E} + \frac{1}{H} \tag{2.26}$$

2.4.2 Multilinear isotropic hardening model

Mróz proposed a material model which describes the plastic response of the material as a multiple linear response. In this model, the plastic region is built up by a superposition of several linear sections. A hardening modulus for each linear section can be defined in the same manner as the bilinear elasto-plastic material model. The Mróz model can be used to describe material behaviour under both static and cyclic loading. [1]

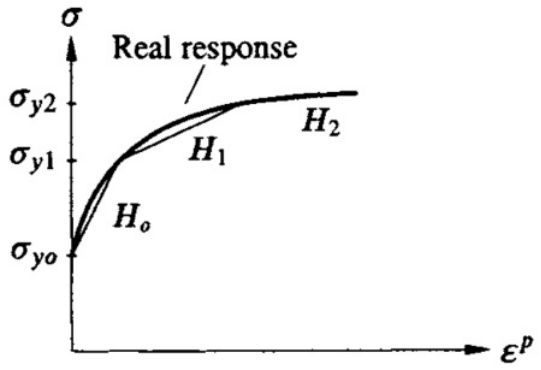

Figure 2.5: An example of a multilinear material model curve [1].

Since it is an isotropic hardening model, the yield criterion is defined by von Mises.

2.4.3 Johnson-Cook

When describing the material behaviour of a metal experiencing plastic strain, one of the most frequently used models is the Johnson-Cook model ([9] to [13]). It accounts for both kinematic strengthening and adiabatic heating of the material. Thus, it is recommended when modeling cases with high strain, strain rates, strain hardening, and non-linear material properties. The effective stress according to the Johnson-Cook material model is generally formulated as,

$$\sigma_{eff} = \left[A + B \cdot (\varepsilon^p_{eff})^n\right] \cdot \left[1 + C \cdot ln\Big(\frac{\dot{\varepsilon}^{vp}_{eff}}{\dot{\varepsilon}_0}\Big)\right] \cdot \left[\frac{T - T_{room}}{T_{melt} - T_{room}}\right]^m \tag{2.27}$$

where ε^p_{eff} is the effective plastic strain, $\dot{\varepsilon}^{vp}_{eff}$ is the effective viscoplastic strain rate, T_{room} is the room temperature, T_{melt} is the melting temperature and the parameters A, B, n, C, $\dot{\varepsilon}_0$ and m are determined through experiments.

A von Mises yield surface together with the isotropic hardening (2.13) is used for this model. In the case of quasi-static loading, the stress associated with the model (2.27) is reduced to,

$$\sigma_{eff} = \left[A + B \cdot (\varepsilon^p_{eff})^n\right] \tag{2.28}$$

At room temperature, $m = 0$ and the parameter A is the yield strength value, designated as $R_{0.2}$. Isotropic strengthening during strains is described with B and n. These parameters called the strain hardening constant, B, and the strain hardening coefficient, n, are determined based on quasi-static data. [8]

2.5 Rate-dependent constitutive relation

For many materials, an increase in yield stress is observed as strain rates increase. Employing the Perzyna formulation given by (2.22), these viscous effects can be included in the aforementioned material models. Consequently, when using explicit dynamic analysis in Abaqus, strain-rate effects need to be added in the material models. Two of the most common material models applied for steels at high strain rates are: Cowper-Symonds and Johnson-Cook [14].

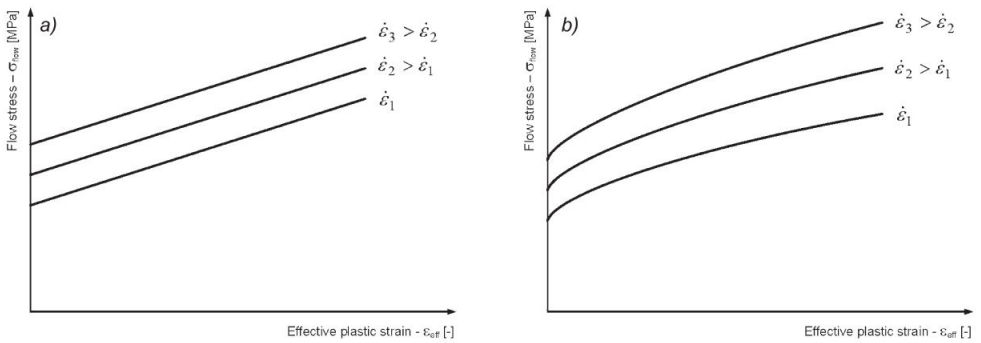

Figure 2.6: Flow stress for a) Cowper-Symonds material model and b) the Johnson-Cook material model [15].

In common, they both predict higher flow-stress curves for larger strain rates according to Fig. 2.6. The main difference lies in how strain-rate effects are accounted for. Consequently, the plastic stress-strain in relation to the strain-rate effects is described with different sets of material parameters. One can observe that C-S material parameters predict parallel curves, as opposed to J-C material parameters where the curves are non-linearly. The reasons for this will be further explained in the following sections.

Previously, the yield surface in the static case was formulated in Eq. (2.8). For a dynamic case, a modification is made such that the dynamic yield surface is defined as,

$$f^d = f - \varphi, \qquad \text{where} \quad \varphi = \varphi\Big(\eta\dot{\varepsilon}^{vp}_{eff}\sqrt{\frac{2}{3}\frac{\partial f}{\partial \sigma_{ij}}\frac{\partial f}{\partial \sigma_{ij}}}\Big) \tag{2.29}$$

Use of the von Mises formulation (2.13) in (2.22) gives,

$$\dot{\varepsilon}^{vp}_{ij} = \frac{\Phi(f)}{\eta}\frac{3s_{ij}}{2\sigma_{eff}} \tag{2.30}$$

The dynamic yield function for an isotropic hardening von Mises formulation can be expressed as,

$$\sigma_{eff} = \sigma_{y0} + K(\varepsilon^{vp}_{eff}) + \varphi(\eta\dot{\varepsilon}^{vp}_{eff}) \tag{2.31}$$

where the effective plastic strain rate $\dot{\varepsilon}^{vp}_{eff}$ and the inverse function φ are obtained as,

$$\dot{\varepsilon}^{vp}_{eff} = (\frac{2}{3}\dot{\varepsilon}^{vp}_{ij}\dot{\varepsilon}^{vp}_{ij})^{1/2}, \qquad \varphi(\Phi(f)) = f \tag{2.32}$$

In Eq. (2.31), the internal variable κ is chosen as $\kappa = \varepsilon^{vp}_{eff}$.

2.5.1 Cowper-Symonds rate dependency

The Cowper-Symonds power law describes the rate-dependence of the material by the following equation,

$$\frac{\sigma^d_{y0}}{\sigma_{y0}} = 1 + \Big(\frac{\dot{\varepsilon}^{vp}_{eff}}{D}\Big)^{1/p} \tag{2.33}$$

where σ^d_{y0} is the dynamic initial yield stress at a plastic strain rate $\dot{\varepsilon}^{vp}_{eff}$, σ_{y0} is the static initial yield stress and D and p are the Cowper-Symonds parameters. D is usually chosen as the reference strain rate in order to make the term $\dot{\varepsilon}^{vp}_{eff}/D$ dimensionless. In Eq. (2.33) the strain-rate modifies the yield stress and does not effect the slope of the curve after yielding (see Fig. 2.6). Comparison of Eq. (2.31) with Eq. (2.33) and by choosing $K(0) = 0$ at

initiation of viscoplasticity lead to,

$$\varphi(\eta\dot{\varepsilon}^{vp}_{eff}) = \sigma_{y0}\Big(\frac{\dot{\varepsilon}^{vp}_{eff}}{D}\Big)^{1/p} \tag{2.34}$$

Using the inverse function φ in (2.34) and adopting $\Phi(f) = \eta\dot{\varepsilon}^{vp}_{eff}$ lead to,

$$\frac{\Phi(f)}{\eta} = D\Big(\frac{f}{\sigma_{y0}}\Big)^{p} = \dot{\varepsilon}^{vp}_{eff} \tag{2.35}$$

which shows how the factor $\frac{\Phi}{\eta}$ in (2.22) is chosen for the Cowper-Symonds model. After initial yield stress is exceeded, i.e. $K = K(\varepsilon^{vp}_{eff})$, the above equation is rewritten to solve a yield function according to Cowper-Symonds,

$$f = \big[\sigma_{y0} + K(\varepsilon^{vp}_{eff})\big] \cdot \Big(\frac{\dot{\varepsilon}^{vp}_{eff}}{D}\Big)^{1/p} \tag{2.36}$$

Use of Eq. (2.13) results in,

$$\sigma_{eff} = \big[\sigma_{y0} + K(\varepsilon^{vp}_{eff})\big]\left[1 + \Big(\frac{\dot{\varepsilon}^{vp}_{eff}}{D}\Big)^{1/p}\right] \tag{2.37}$$

Comparison with (2.33) concludes that the static yield stress is,

$$\sigma_{st}(\varepsilon^{vp}_{eff}) = \big[\sigma_{y0} + K(\varepsilon^{vp}_{eff})\big] \tag{2.38}$$

which can be used to fit experimental data.

2.5.2 Johnson-Cook rate dependency

With the empirical Johnson-Cook model, strain-rate effects are taken into account with the second parentheses in Eq. (2.27). The dynamic initial yield stress can be formulated such that it depends on the static initial yield stress as,

$$\sigma_{y0}^{d} = \sigma_{y0}\left[1 + C \cdot ln\Big(\frac{\dot{\varepsilon}_{eff}^{vp}}{\dot{\varepsilon}_0}\Big)\right] \tag{2.39}$$

where the initial static yield stress is $\sigma_{y0} = A = R_{0.2}$. At initiation of viscoplasticity, the hardening parameter is set to $K(0) = 0$ which reduces Eq. (2.31) to $\sigma_{eff} = \sigma_{y0} + \varphi(\eta\dot{\varepsilon}_{eff}^{vp})$. A comparison is made with (2.39) to give,

$$\varphi(\eta\dot{\varepsilon}_{eff}^{vp}) = \sigma_{y0}C \cdot ln\Big(\frac{\dot{\varepsilon}_{eff}^{vp}}{\dot{\varepsilon}_0}\Big) \tag{2.40}$$

Using the definition of the inverse function, φ given in Eq. (2.32) and adopting $\Phi(f) = \eta\dot{\varepsilon}_{eff}^{vp}$ lead to,

$$f = \sigma_{y0}C \cdot ln(\frac{\Phi(f)}{\eta\dot{\varepsilon}_0}) \tag{2.41}$$

Rearrangement shows how the factor $\frac{\Phi(f)}{\eta}$ in (2.22), is chosen for the Johnson-Cook model,

$$\frac{\Phi(f)}{\eta} = \dot{\varepsilon}_0 \exp\left(\frac{f}{\sigma_{y0}C}\right) = \dot{\varepsilon}_{eff}^{vp} \tag{2.42}$$

Beyond the initial yield stress, the yield function is solved from the above equation to

$$f = \big[\sigma_{y0} + K(\varepsilon_{eff}^{vp})\big]C \cdot ln\Big(\frac{\dot{\varepsilon}_{eff}^{vp}}{\dot{\varepsilon}_0}\Big) \tag{2.43}$$

Use of Eq. (2.13) where the internal variable is chosen as $\kappa = \varepsilon_{eff}^{vp}$, results in

$$\sigma_{eff} = \big[\sigma_{y0} + K(\varepsilon_{eff}^{vp})\big]\left[1 + C \cdot ln\Big(\frac{\dot{\varepsilon}_{eff}^{vp}}{\dot{\varepsilon}_0}\Big)\right] \tag{2.44}$$

Comparison with Eq. (2.27) at room temperature, and the definition of the Johnson-Cook parameters B and n concludes that $K(\varepsilon_{eff}^{vp}) = B \cdot (\varepsilon_{eff}^{vp})^n$.

Now, the remaining parameters in the J-C model, that takes strain-rate effects into account are treated as follows. To start, a reference strain rate is set as $\dot{\varepsilon_o}$, normally as a quasi-static strain rate. Its role is to make the time units in the strain-rate term non-dimensional [17]. Later, when other experiments are made with different strain rates, the strain rate sensitivity coefficient, C can be assessed. This accounts for kinematic strengthening, i.e. strain intensity effects. Manually fitting the parameter would then be according to the following equation,

$$C = (\sigma_2/\sigma_1 - 1)/(ln(\dot{\varepsilon_2}/\dot{\varepsilon_0}) - \sigma_2 \cdot ln(\dot{\varepsilon_1}/\dot{\varepsilon_0})/\sigma_1). \tag{2.45}$$

3 Experiment

3.1 Introduction

The most common experiment used to understand mechanical behaviour of materials is the *tensile test*. A tensile test can be done either uni-axial or bi-axial. For the case of uni-axial tensile test, which is typically used for isotropic materials, the force is applied in one direction to obtain mechanical properties. This is done by pulling one end of the specimen, while the other end remains fixed. Whereas bi-axial applies force in two directions and is used for anisotropic materials.

The result of a tensile test is a curve showing how the specimen reacts to the applied loading conditions. Fig. 3.1 illustrates a typical force-displacement diagram for a tensile test on a sheet steel specimen. The elastic extension is very small compared to the total extension. One characteristic is the initial yielding load, F_y, at which plastic deformation starts to occur. Following the initial yielding is a region where load increases due to strain-hardening which is a phenomenon that exhibits by most metals and alloys. [4]

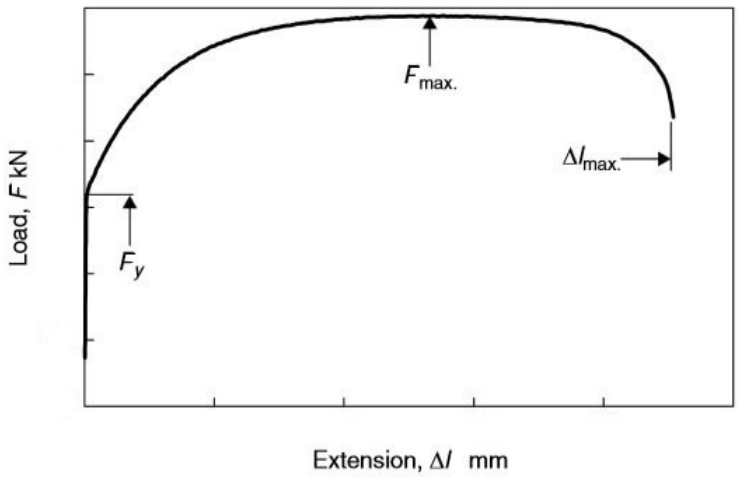

Figure 3.1: A typical force-displacement diagram for a tensile test of sheet steel [4].

In order to obtain mechanical properties of a material, a stress-strain curve needs to be formed. The program that is used to obtain the data scales the load-extension diagram in a manner that will be presented in the following steps [2].

The nominal or engineering stress is defined as the load divided by the initial cross-sectional area,

$$\sigma_n = \frac{F}{A_0} \tag{3.1}$$

The convectional or engineering strain is represented by,

$$\varepsilon = \frac{l - l_0}{l_0} \tag{3.2}$$

where l_0 and l are the initial and current gauge length respectively. The engineering stress and strain are not accurate, since the changes of the cross-sectional area and the gauge length with load are not considered. Assuming the volume of the specimen remains constant,

$$A_0 l_0 = Al \tag{3.3}$$

The true stress can now be defined as the load divided by the current area (the changing

area with respect to time),

$$\sigma = \frac{F}{A} = \frac{Fl}{A_0 l_0} \tag{3.4}$$

The true stress can also be expressed in terms of the engineering stress and strain. Insertion of (3.1) and (3.2) in (3.4), gives the relation between the true and engineering stress,

$$\sigma = \sigma_n(1 + \varepsilon) \tag{3.5}$$

The increment of the strain has the following relation,

$$d\bar{\varepsilon} = \frac{dl}{l} \tag{3.6}$$

Integration of (3.6) from the initial length to the length l gives,

$$\bar{\varepsilon} = \int_{l_o}^{l} \frac{dl}{l} = ln\frac{l}{l_0} \tag{3.7}$$

The true strain can be obtained using the engineering strain by using (3.2) in (3.7),

$$\bar{\varepsilon} = ln(1 + \varepsilon) \tag{3.8}$$

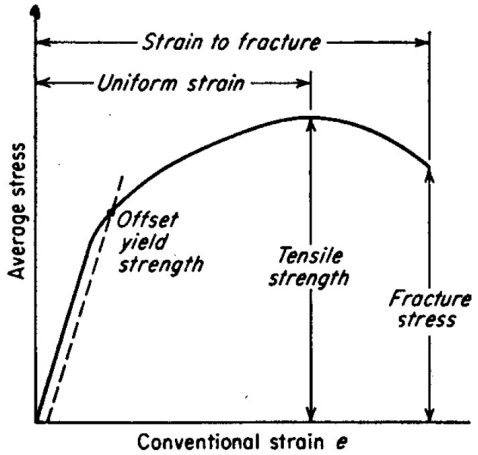

Figure 3.2: A typical stress- strain curve for metals.

In Fig. 3.2, a typical stress-strain curve is observed. The slope in the elastic region is expanded for a clearer view of the displayed material properties. One of which is a measure of elastic stiffness called the Young's modulus. It is defined as a ratio of stress-strain curve in the elastic region. This mechanical property can be calculated as,

$$E = \frac{\Delta\sigma}{\Delta\varepsilon} \tag{3.9}$$

Following the calculation of the Young's modulus, the yield strength σ_y, is found as displayed in Fig. 3.2. The slope of the Young's modulus is used to construct a parallel line with an offset in the positive x-axis by 0.2%. It is necessary to construct since some materials do not display a sharp transition between the elastic and plastic region.

3.2 Material

The tubes used in Tetra Pak's processing equipment are made of stainless steel 316L. In some manufacturing steps, a deformation is done on the tubes to change the geometry. The material proves great corrosion resistance and is commonly used in industries such as food processing. The tubes are welded and heat treated. The material composition provided by the material producers, is given in Table 3.1. .

Table 3.1: Chemical composition of Stainless Steel 316L

	C	Si	Mn	P	S	Cr	Mo	Ni	N	Ferz
Composition (%)	0,028	0,53	0,87	0,035	0,0010	17,00	2,03	10,10	0,032	8,3

3.3 Tensile test procedure

Before performing the tensile test, the specimen geometry had to be defined. This was chosen according to ASTM E8/E8M standard as specified in Table 3.2. Once the geometry was defined, a drawing of the test specimen was created using *Creo Parametric*. At Tetra Pak, a water jet cutting process could then be used to prepare the specimens from sheet plates with a thickness of 0.8 m.

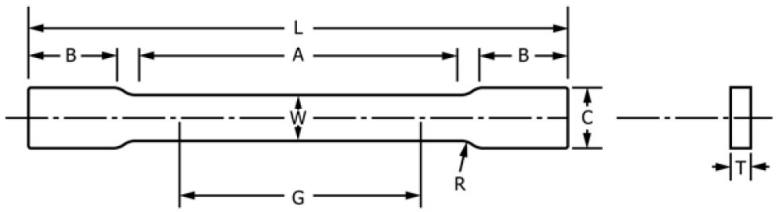

Figure 3.3: Specimen geometry

Table 3.2: Dimensions of specimen according to ASTM E8/E8M standards

Description	Dimensions [mm]
Thickness (T)	0.8
Width (W)	4.2
Gauge length (G)	21.0
Radius of fillet (R)	3.49
Sample length (L)	45.5
Parallel length (A)	23.625
Grip length (B)	7.5
Grip width (C)	10

In this study, uni-axial tensile tests were performed using Instron ElectroPuls^{TM} E10kN (bi-axial), housed at Lund University. A software, called *Bluehill*, was also used as part of the testing method.

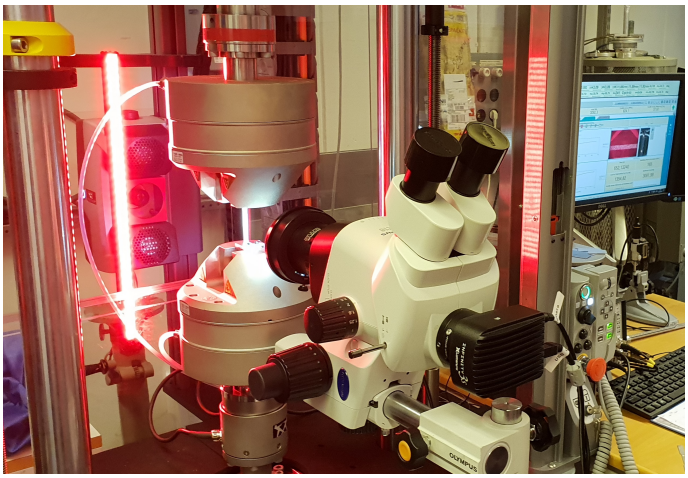

Figure 3.4: The testing set-up

As seen in Fig. 3.4, the specimen was fixed with two vertically aligned pneumatic clamps. Before the specimen was tested, the initial dimension of the cross-sectional area was measured using a digital micrometer. Two white dots were also marked on the specimen (see Fig. 3.5) representing the gauge length, G, given in Table 3.2. Afterwards, the specimen was mounted in the clamps. A video extensometer was used to monitor the change in gauge length.

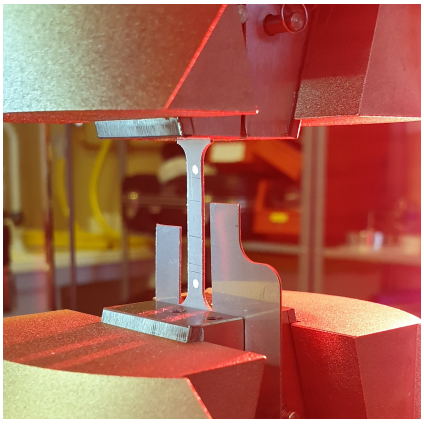

Figure 3.5: The specimen loaded into the clamps

The machine works by pulling the upper clamp (called *crosshead*) at a speed, v, as given in Table 3.3, while maintaining the bottom clamp stationary. This continued until the specimen broke. After breaking, the specimen was removed from the machine and the final

dimensions of the cross-sectional area were measured. At the end of the test, the software produced an excel file containing the results. These results included the following,

- *Force [N]* - Reaction force measured by the load cell
- *Extension [mm]* - Extension of the clamps
- *Engineering stress [MPa]* - Calculated by a software using Eq. (3.1)
- *Engineering strain [mm/mm]* - Measured by the video extensometer

The true stress and strain values were then calculated using Eq. (3.2) and Eq. (3.1). This data was then used to determine material properties of 316L, according to Section (3.1). The tensile tests were conducted for 9 samples at room temperature. The mechanical behaviour of the material was investigated under quasi-static loading. The quasi-static tests were performed according to the standard ISO 6892-1 [16] at a strain rate of 10^{-3} s^{-1} to obtain material properties, such as Young's modulus and yield stress. The dynamic testing standard used is named ISO 26203-2 [16]. There were limitations when performing tensile tests at higher strain-rates, resulting in inaccurate data. Due to that, a low range of strain-rates were performed to study the material behaviour under dynamic conditions, namely 10^{-2} s^{-1} and $5 \cdot 10^{-2}$ s^{-1}. The velocities and strain-rate values are summarized in the table below,

Table 3.3: Displacement rates corresponding to the different strain rates

Test type	Quasi-static	Dynamic	Dynamic
$\dot{\varepsilon}_p$ $[s^{-1}]$	10^{-3}	10^{-2}	10^{-2}
v [mm/s]	0.021	0.21	1.05

To investigate the value of the Young's modulus, a test was conducted for a specimen with a larger dimension, shown in Table 3.4.

Table 3.4: Dimensions of specimen according to ASTM E8/E8M standards

Description	Dimensions [mm]
Thickness (T)	0.8
Width (W)	12.5
Gauge length (G)	50
Radius of fillet (R)	12.5
Sample length (L)	200
Parallel length (A)	57
Grip length (B)	50
Grip width (C)	20

In this case, a mechanical extensometer was used to ensure accurate extension measurement. The extensometer was connected to the specimen as in Fig. 3.6.

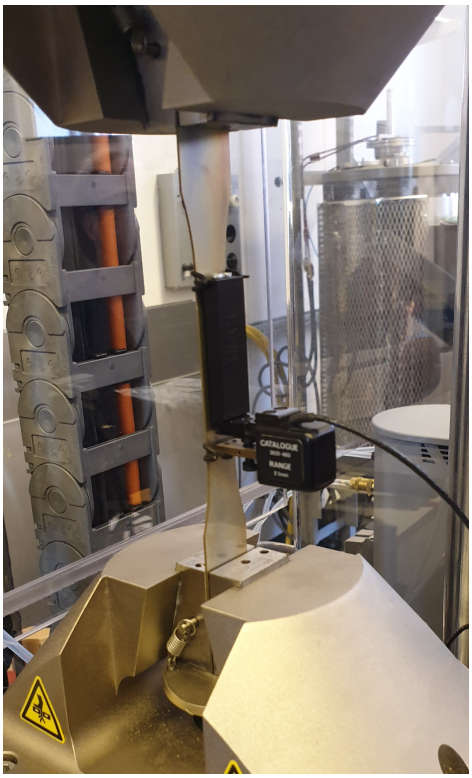

Figure 3.6: Mechanical extensometer connected to the specimen

4 Finite Element Analysis

The finite element analysis (FEA) is a numerical method used to solve physical problems that are described by partial differential equations [19]. A model of the physical problem is set up in an FE-program to simulate and analyze the model. The applications for this method are wide, some models are linear, others are non-linear. FE-models can be used for both static and dynamic analyses. For this study, the application is to study material non-linearity and the dynamics at different strain rates. Solving non-linear problems by finite element method involves modeling, describing the problem with a set of non-linear equations and using an iterative procedure to solve the problem [5]. Modeling and analysis of a physical problem include the following steps [7]:

1. Preprocessing - material properties, element type, mesh, boundary conditions and load conditions are defined.

2. Simulation - solving the numerical problem.

3. Postprocessing - visualization and interpretation of results.

These three steps are explained in more details in this chapter.

4.1 Preprocessing - set up of a virtual tensile test

Preprocessing is the initial step to analyze a physical problem. For that, a preprocessor is used for creating geometries, setting up boundary conditions, defining material properties and other necessary specifications that will mimic the physical problem. The preprocessor

that was provided for this study is called HyperMesh, which is a package within the software HyperWorks. Its function is not to solve the problem, but to generate an input file (.inp) that can be interpreted by a solver to run the simulation. For this study, the input files were created to be compatible with the Abaqus/Explicit solver.

To start, the specimen was created as a solid with the same geometry as in the experiment. Next, a mesh consisting of solid elements of type C3D8R, (Continuum 3D, hexahedron/8 nodes, reduced integration) was constructed onto the solid. Finer mesh was desired in the region where stresses were assumed to be concentrated, i.e. the gauge length region. Whereas the remaining region, especially at the ends of the specimen, was constructed with a coarser mesh to reduce simulation time.

As seen in Fig. 4.1, only half of the specimen was modelled. This is because the problem allows use of symmetry constraints. Each element needs to be solved later with a set of non-linear equations, therefore, a benefit of using symmetry is that a reduced model results in reduced computational time. The symmetry constraints are described by boundary conditions at a surface that lies on the symmetry plane. The nodes on this surface are not allowed to translate normal to the surface nor rotate about the axis of the symmetry plane. Thus, the expected deformation would also be symmetrical.

Figure 4.1: Simulation model using symmetry constraints

Apart from symmetry constraints, only the domain of the specimen in-between the clamps was analyzed. Thus, a reduction in length of the model was also made possible. The

loading conditions were applied in the same manner as in the physical tensile test. That is, one end of the specimen was fixed while the other end was subjected to a prescribed displacement. For the fixed end, all the nodes at the bottom surface were prescribed fixed (see Fig. 4.2).

For the other end, a so-called multi-point constraint (MPC) was used, which allows constraints to be imposed between different degrees of freedom [6]. Here, one node that is defined away from the model is chosen as a master node and is only allowed to move longitudinally. It is connected using a multi-point-constraint (MPC) to a set of nodes on the upper surface, the connection is seen as green lines in Fig. 4.1. A constant displacement rate, v, as specified in Table 3.3, is then given to the MPC master node and all the connected nodes will behave accordingly. To obtain strain measurements, the gauge length was defined with two node sets in the same region and the same length as in the physical tensile test.

Figure 4.2: Zoomed view of model

The next step was to assign material properties to the model. These material properties were defined with the same values as obtained from the physical tensile test. Since isotropic elastic behaviour was assumed, the elasticity was defined with the calculated Young's modulus and Poisson's ratio was assumed to be 0.3. When this was done, an input file from HyperMesh was created and further material model definitions could be made manually

in the file. For each material model, the plastic part was defined with values obtained from calibration with respect to test data. The simulation time was defined, which was calculated as

$$t = \frac{\Delta}{\mathrm{v}}$$

where Δ, is the displacement and v, the displacement rate according to Table 3.3. Some of the additional outputs listed below, were also added in the input file:

- History outputs
  - U2 - displacement in the y-direction. One for the MPC master node and two for the gauge points
  - RF2 - reaction force in the y-direction for the MPC master node
- Global field outputs
  - PEEQ - equivalent plastic strain as Eq. (2.21)
  - S - all stress components, including the von Mises effective stress as Eq. (2.11)
  - ER - all logarithmic strain rate components, including the effective plastic strain rate as Eq. (2.20)

In the input file, the specification of how often these outputs would be requested was also defined.

4.2 Material models and calibration

Material models were picked in consideration of what was available in Abaqus. The ones that were suitable for this case were discussed in Chapter 2. The implementation of each of the models will now be presented.

4.2.1 Rate independent material model

Current bilinear model implementation

The already existing bilinear material model was implemented with an elastic part defined with a Young's modulus of 200 GPa and Poisson's ratio of 0.3. Two pairs of plastic stress-strain values were used to defined the plastic region. These pairs were provided by Tetra Pak as listed in Table 4.1.

Table 4.1: Calibrated plastic stress-strain values for the current bilinear model.

Stress [MPa]	Plastic strain
265	0
605	0.66

Bilinear model implementation

Implementation of this material model in Abaqus required defining an elasticity modulus and two pairs of plastic stress-strain values. A Young's modulus of 200 GPa was used for the linear elastic region up to the yield stress. For plasticity, two pairs of plastic stress-strain values were used (see Table 4.2). The first pair was defined as the initial yield stress with a plastic strain of zero. The tangent modulus was determined using curve fitting in Matlab. Inserting the Young's and tangent modulus into relation (2.26), the hardening modulus was obtained. Since the hardening modulus is the slope of plastic stress-strain, the stress value for the second pair was calculated using this modulus for a plastic strain of 0.6 mm/mm.

Table 4.2: Calibrated plastic stress-strain values for the bilinear model.

Stress [MPa]	Plastic strain
275	0
1392.8	0.6

Multilinear model implementation

The multilinear model was fitted by selecting points along the tensile curve in the plastic region. The tangent modulus at each linear section were calculated and used in Eq. (2.26) to obtain the hardening modulus. The point selection was denser at the elasto-plastic region and sparser at higher stress value (see Fig. 4.3).

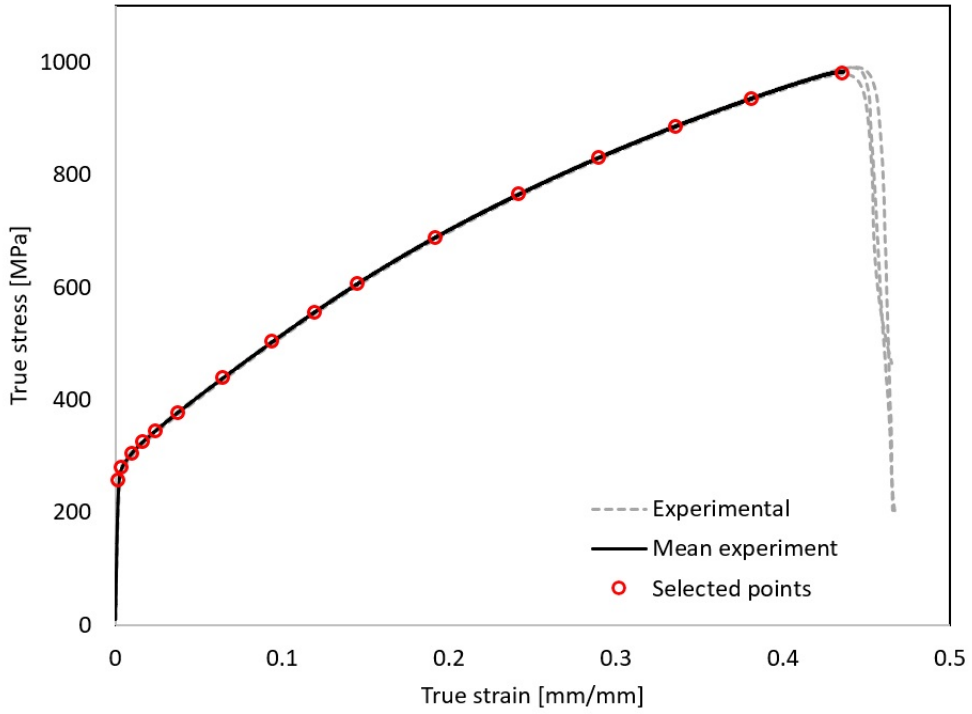

Figure 4.3: Pairs of plastic stress-strain values for the multilinear model demonstrated as red circles on the experimental curve.

For the elastic part, the same value for Young's modulus was used. This material model was built up by 17 plastic stress-strain points as shown in Table 4.3.

Table 4.3: Pairs of plastic stress-strain values for the multilinear model.

Stress [MPa]	Plastic strain
256.73	0
279.62	0.0020
305.09	0.0080
325.69	0.0148
344.21	0.0219
377.02	0.0355
438.73	0.0628
502.79	0.0922
555.43	0.1174
605.71	0.1431
688.73	0.1902
764.78	0.2399
829.34	0.2875
885.64	0.3339
935.08	0.3792
980.82	0.4333
1134.19	0.598

Johnson-Cook model implementation

The elastic part was defined in the same manner as the previous material models. For the plastic part, the Johnson-Cook model (2.28) involves several material parameters that need to be calibrated against results from experimental data. Since the experiment was done in room temperature, m is set to zero. Moreover, the parameter A is set as the initial yield, i.e. $A = R_{0.2}$, obtained from the quasi-static data. The remaining parameters B and n are established by a curve fitting tool in Matlab. The results from curve fitting are seen in Table 4.4.

Table 4.4: Calibrated quasi-static parameters for Johnson-Cook model.

Material	A [MPa]	B [MPa]	n
316L	275	1356	0.7344

4.2.2 Rate-dependent material model

Cowper-Symonds

To determine Cowper-Symonds parameters D and p, Eq. (2.37) was used to fit the experimental data. The results are presented in Table 4.5. These values are only valid for strain-rates showed in Table 3.3.

Table 4.5: Calibrated Cowper-Symonds parameters

D	p
10^{-3}	1.465

Using these values with higher strain-rates will result in an overestimated prediction of yield stress. The parameters could not be calculated correctly due to the limitation of performing tensile test at higher strain-rates with the current tensile testing machine. In order to determine the C-S parameters accurately, other experimental techniques such as Taylor test and Split Hopkinson Pressure Bar should be used. Unfortunately, they were not available for this study.

Johnson-Cook

The rate dependency is important to implement at higher strain rates since it has an impact on the yield stress. In Johnson-Cook, the selection of the strain-rate normalization parameter, $\dot{\varepsilon_0}$ can be done in two ways. It is important to be consistent with the choices of the parameters A and B when selecting $\dot{\varepsilon}_0$. If the parameters A and B are determined from quasi-static data, then $\dot{\varepsilon}_0$ should be set to the value of the effective plastic strain-rate used in the quasi-static test: $\dot{\varepsilon}_0 = \dot{\varepsilon}^p_{eff}$. If not, the parameters A and B need to be modified. The selection of $\dot{\varepsilon}_0 = 1s^{-1}$ together with the parameters A and B from quasi-static data is often seen in research, but this misunderstanding underpredicts the static response [17]. After estimating the other J-C parameters, the remaining strain-rate parameter, C was obtained by curve fitting the dynamic tensile test data and an average of C was calculated. Table 4.6 shows the Johnson-Cook parameters employed in this study.

Table 4.6: Calibrated parameters for Johnson-Cook model from dynamic data

Material	A [MPa]	B [MPa]	C	n	$\dot{\varepsilon_0}$ $[s^{-1}]$
316L	275	1356	0.002498	0.7344	10^{-3}

4.3 Simulation

After modeling the problem, an Abaqus/Explicit input file (.inp) was generated. The input file was submitted to Abaqus for solving the numerical problem defined in the model. It was done using an explicit time-integration scheme. The explicit analysis procedure in Abaqus/Explicit uses Euler forward discretization scheme to solve the non-linear problem. During the first phase of the simulation, Abaqus calculates the initial stable time increment which yields the time frame of each iteration, shown in Eq. (4.1).

$$\Delta t \leq \frac{2}{\omega_{max}} \tag{4.1}$$

where ω_{max} is the highest eigenvalue in the system. The stable time increment is regularly updated throughout the simulation.

4.4 Postprocessing

Once the FE analysis was completed, Abaqus generated an output file (job.odb) containing the calculated results. These results were displayed using the Visualization module of Abaqus/CAE (Abaqus/Viewer). The field results were displayed on the model and simulation was animated to understand how the specimen was deformed. The history results were then exported as vectors and imported into Excel for plotting.

4.5 Single element test

Before running the non-linear finite element analysis, the material response was controlled using a single element test. For this purpose, an Abaqus/CAE plug-in was provided by Tetra Pak. The single element plug-in consists of an element with the boundary and load condition as shown in Fig. 4.4.

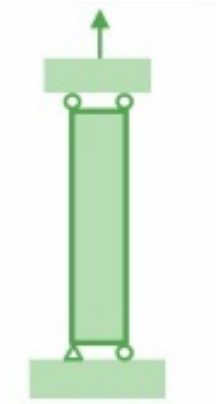

Figure 4.4: Single element test set-up in Abaqus.

The solid element (C3D) was used with the same dimensions as the elements in the model. The tests were performed using an explicit numerical solver.

4.6 Goodness-of-fit

After model fitting, it is important to check how well the model fits the experimental data. It can be measured with the coefficient of determination also known as R-squared [20]. The R^2-value usually ranges between 0 and 1,

- $R^2 = 0$ indicates the model does not properly fit the experimental data.
- $R^2 = 1$ indicates the model fits the experimental data perfectly.

The common expression for R^2 is presented as,

$$R^2 = 1 - \frac{SS_{resid}}{SS_{total}} \tag{4.2}$$

where the sum of the squared residuals, SS_{resid}, and the sum of the squared differences, SS_{total}, are obtained as,

$$SS_{resid} = \sum_i (y_i - f_i)^2, \qquad SS_{total} = \sum_i (y_i - \bar{y})^2, \qquad \bar{y} = \frac{1}{n}\sum_{i=1}^{n} y_i \tag{4.3}$$

y is the model values, $\bar{y}$ the average value of y and f is the experimental values. A Matlab script was written containing Eq. (4.2) and Eq. (4.3) to calculate R^2-value for each fitted model.

5 Empirical Analysis

In this chapter, the results obtained from both tensile testing and postprocessing will be presented. Illustrative comparisons of data from testing and simulations are made using Matlab, whereas Abaqus Viewer is used to capture images of the postprocessing.

5.1 Results

Tensile test results

Results for the material response at the reference strain rate of $10^{-3}\ s^{-1}$ are shown in Fig. 5.1.

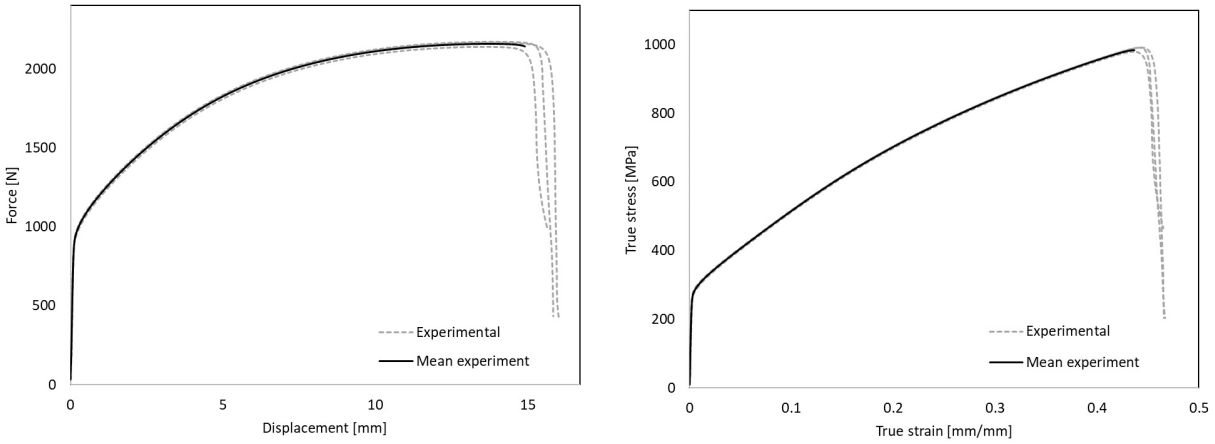

(a) Force-Displacement curve (b) True stress-strain curve

Figure 5.1: Experimental results at a strain rate of $10^{-3}s^{-1}$.

Fig. 5.2 illustrates the experimental results at different strain-rates.

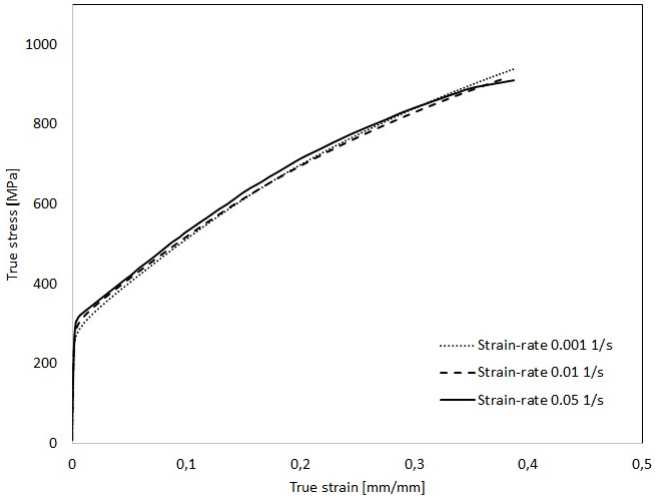

Figure 5.2: Experimental results at different strain-rates.

The yield stress and the Young's modulus for each experiment are determined and presented in the following table,

Table 5.1: Obtained material properties at different strain rates.

Strain rate $[s^{-1}]$	Yield stress [MPa]	Young's modulus [GPa]
10^{-3}	275	200
10^{-2}	287	180
$5 \cdot 10^{-3}$	311	148

The stress variation are plotted with respect to the logarithmic strain-rate for four different strain levels.

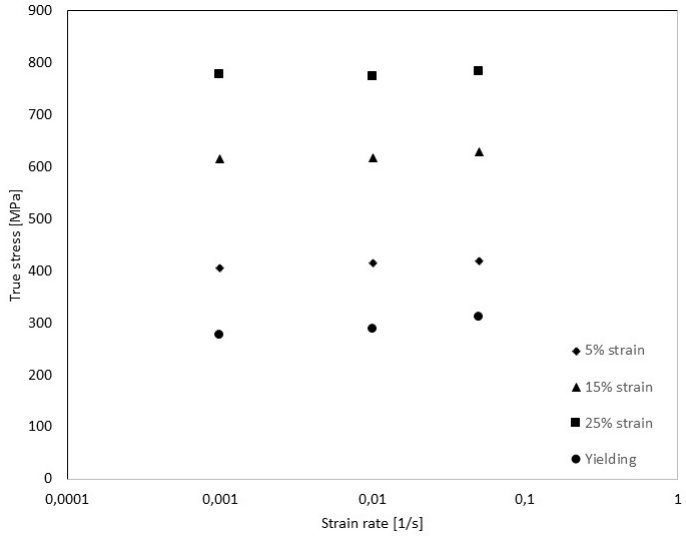

Figure 5.3: The stress variation with respect to the logarithmic strain-rate.

Virtual tensile test results

Calibration of the proposed material models from quasi-static experimental data are presented in Fig. 5.4 - 5.6.

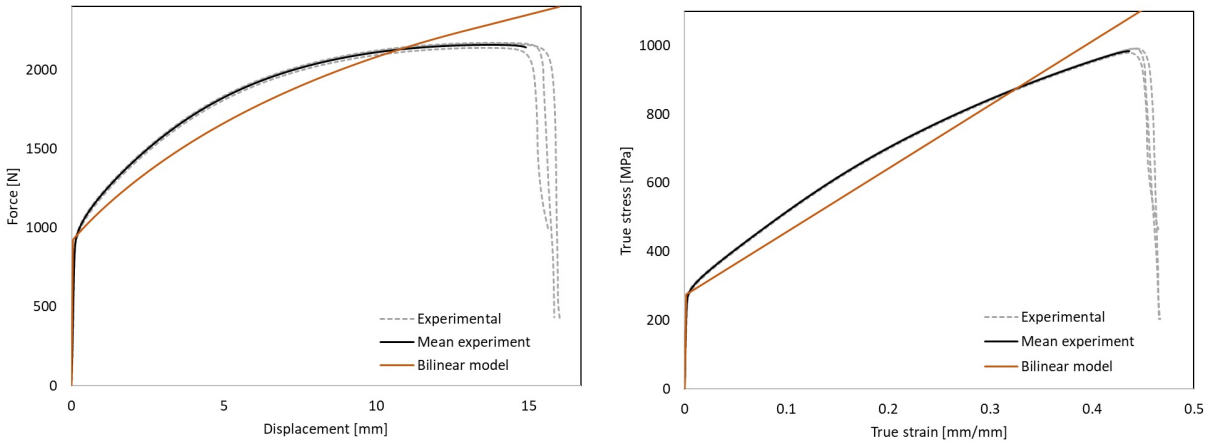

(a) Force-Displacement curve

(b) True stress-strain curve

Figure 5.4: Virtual vs experimental tensile test using bilinear model under quasi-static loading condition.

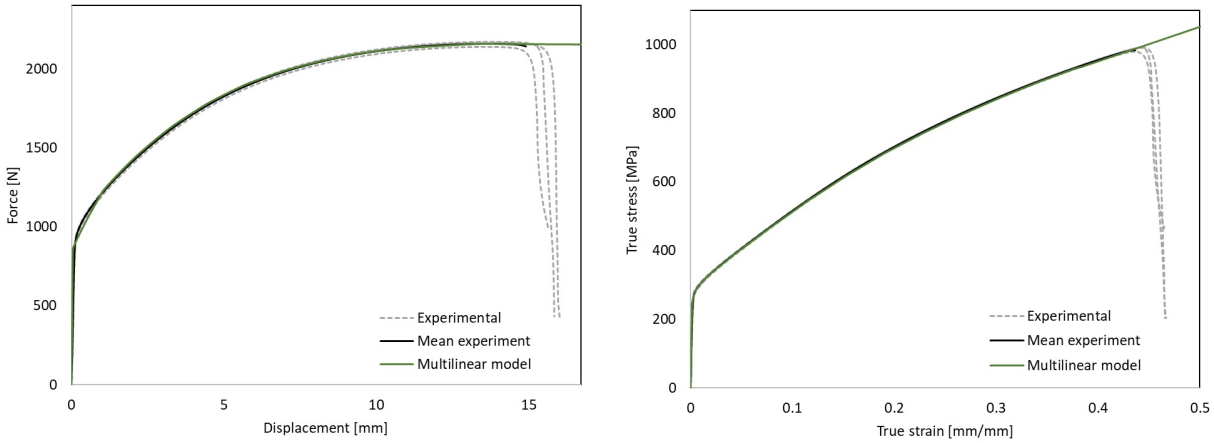

(a) Force-Displacement curve (b) True stress-strain curve

Figure 5.5: Virtual vs experimental tensile test using multilinear model under quasi-static loading condition.

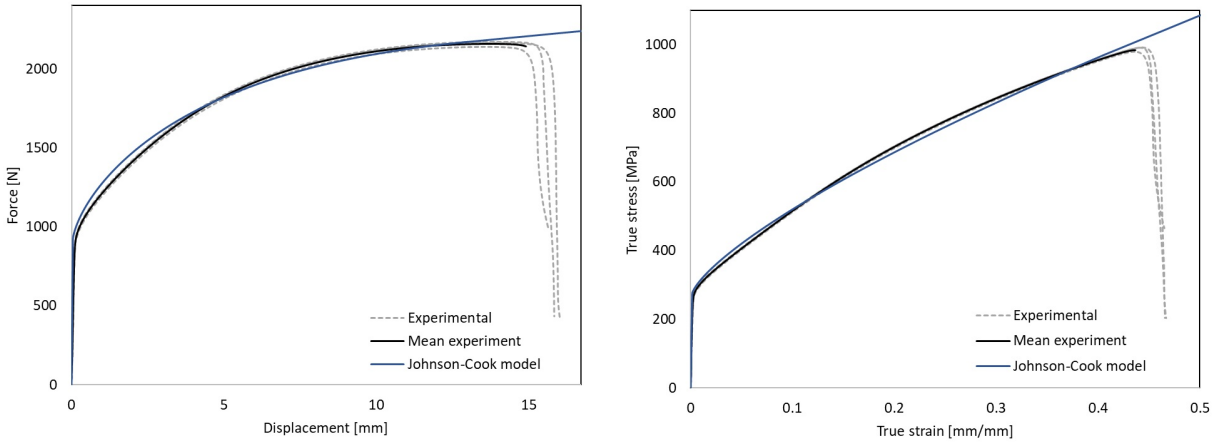

(a) Force-Displacement curve (b) True stress-strain curve

Figure 5.6: Virtual vs experimental tensile test using Johnson-Cook model under quasi-static loading condition.

To better understand how well the materials models fit the experimental curve, the coefficient of determination, R^2-value, is calculated and showed in Table 5.2.

Table 5.2: Calculated R^2-value for the proposed models.

Model	Bilinear	Multilinear	Johnson-Cook
R^2-value	0.9692	0.9935	0.9919

Results from the proposed material models, the current bilinear model and the experimental tests are plotted as stress-strain curves in Fig. 5.7.

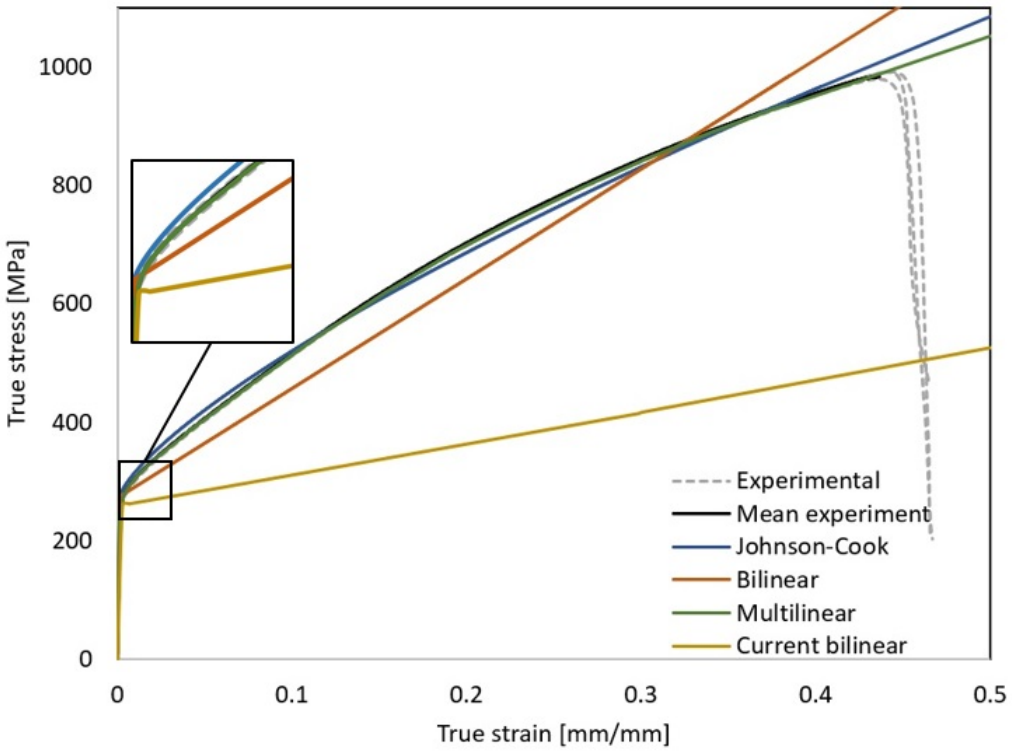

Figure 5.7: A comparison between the experimental values and the different material models.

The effective plastic strain and von Mises stress are displayed as field results on the model and presented in Fig. 5.8-5.11.

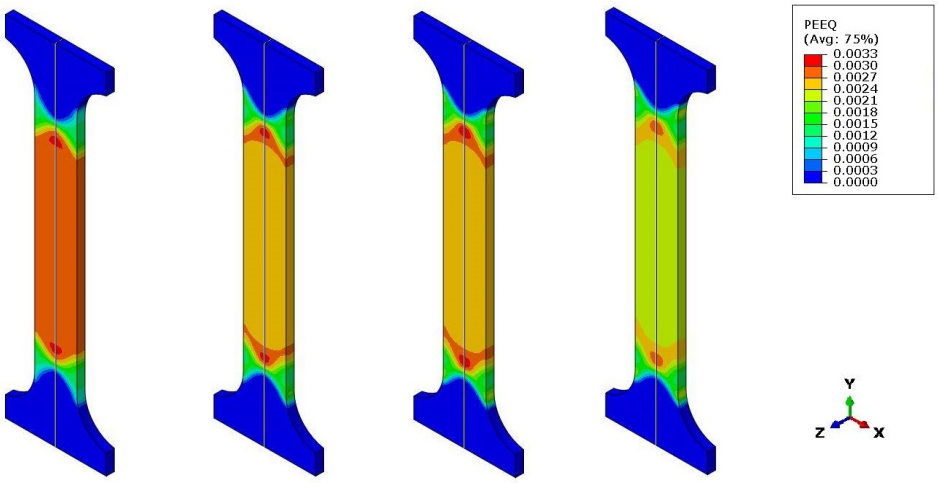

(a) (b) (c) (d)

Figure 5.8: Equivalent plastic strain at 0.1 mm displacement, (a) Current bilinear, (b) Bilinear, (c) Multilinear and (d) Johnson-Cook.

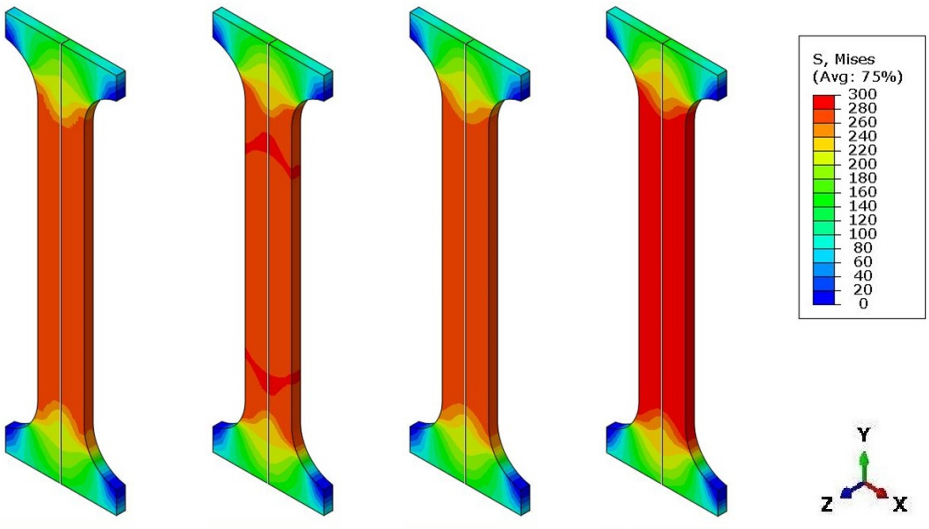

(a) (b) (c) (d)

Figure 5.9: von Mises effective stress at 0.1 mm displacement, (a) Current bilinear, (b) Bilinear, (c) Multilinear and (d) Johnson-Cook.

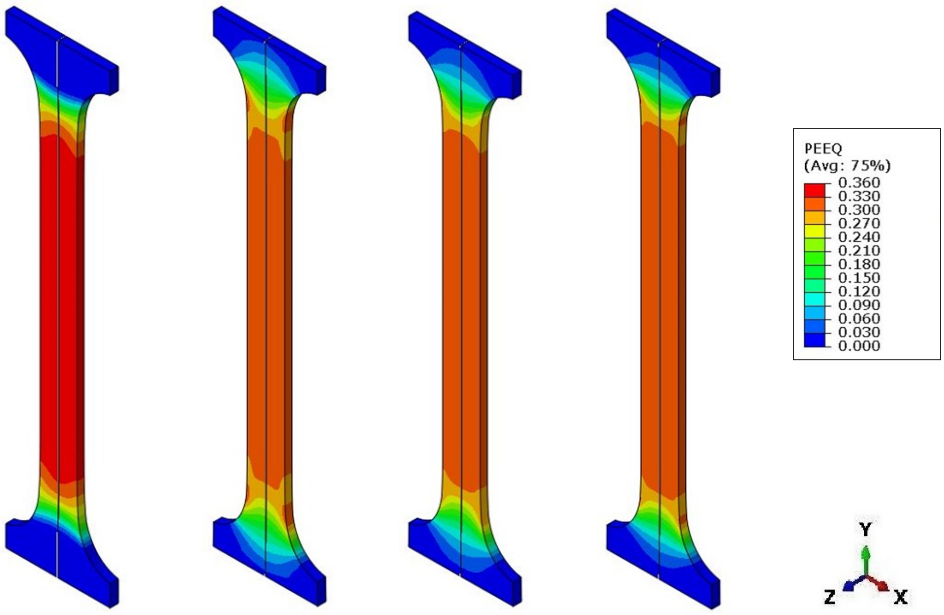

(a) (b) (c) (d)

Figure 5.10: Equivalent plastic strain at 10 mm displacement, (a) Current bilinear, (b) Bilinear, (c) Multilinear and (d) Johnson-Cook.

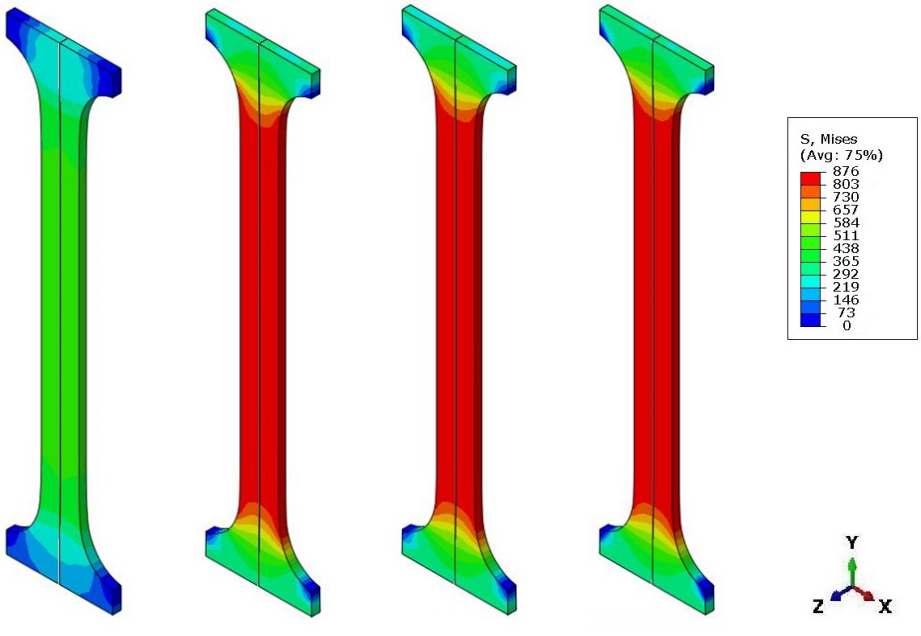

(a) (b) (c) (d)

Figure 5.11: von Mises effective stress at 10 mm displacement, (a) Current bilinear, (b) Bilinear, (c) Multilinear and (d) Johnson-Cook.

Simulation and manufacturing process

The material models were implemented on one application where the tube is deformed. Results from the virtual process are shown in the following figures.

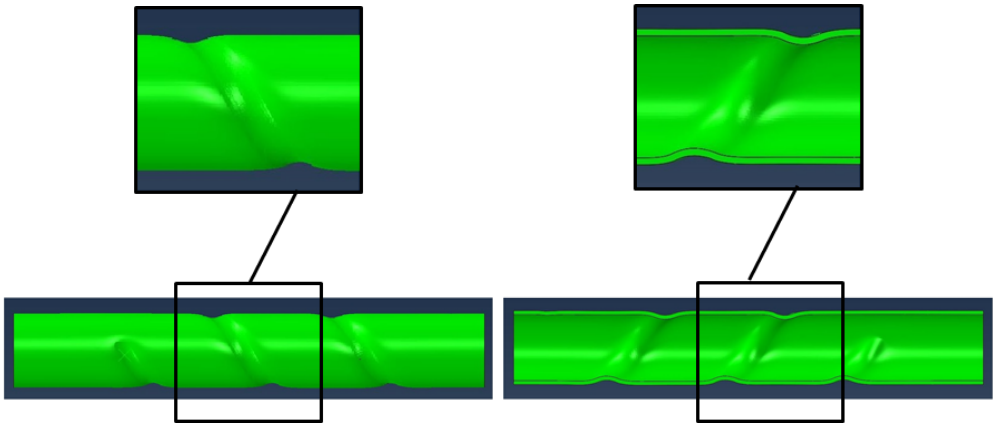

(a) Outside of tube (b) Inside of tube

Figure 5.12: Deformation of the outside and the inside of tube at full step, analyzed region is magnified.

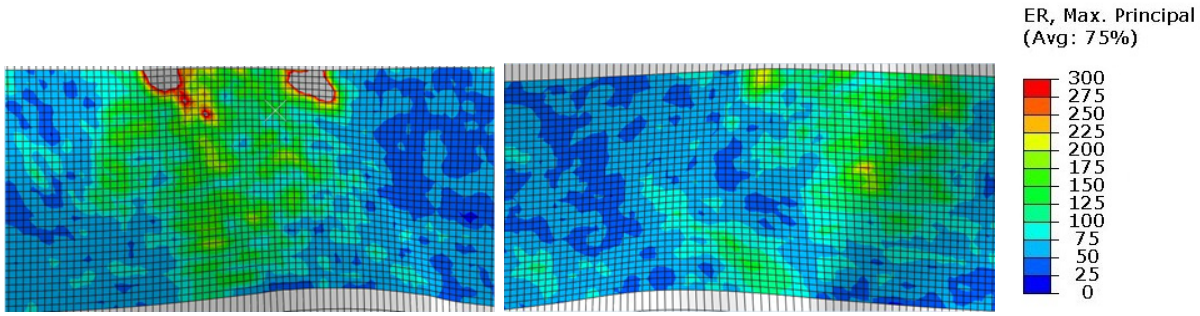

(a) Outside of tube (b) Inside of tube

Figure 5.13: Effective plastic strain-rate for Johnson-Cook material model.

Table 5.3: Equivalent plastic strain for different material models.

Material model	Outside of tube	Inside of tube
Current bilinear	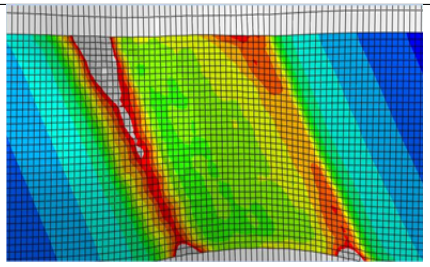	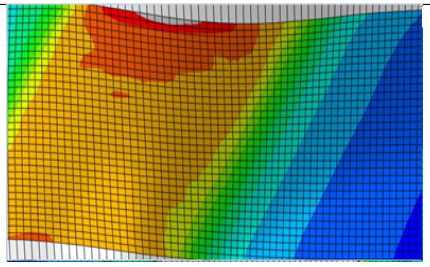
Bilinear	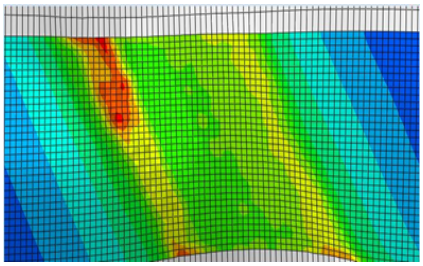	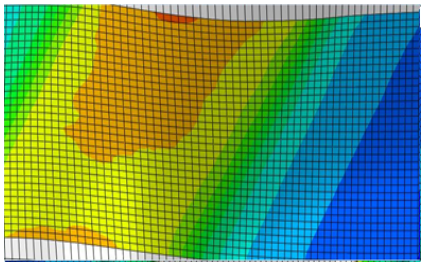
Multilinear	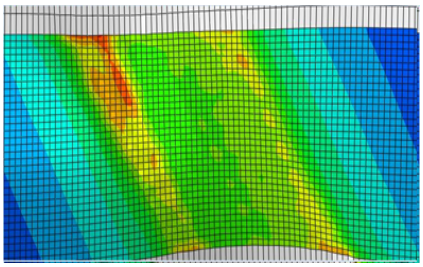	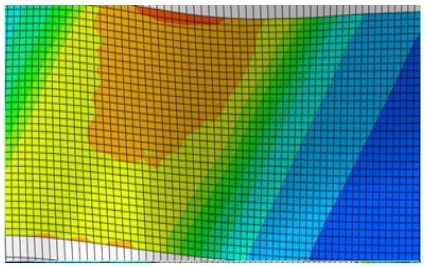
Johnson-Cook	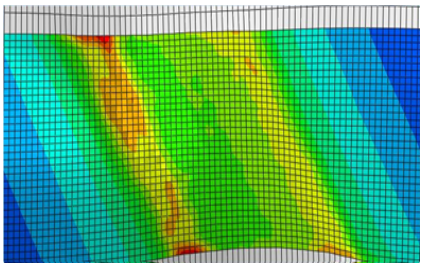	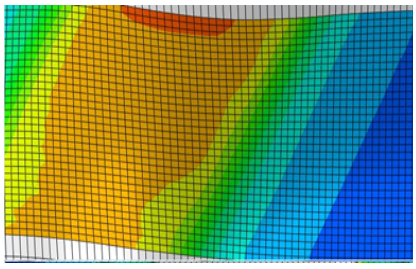

Table 5.4: von Mises effective stress for different material models.

Material model	Outside of tube	Inside of tube
Current bilinear	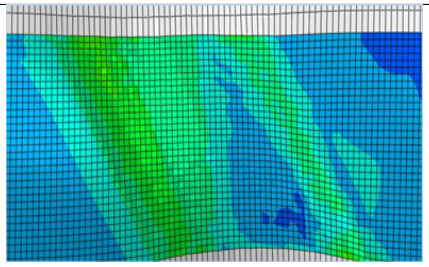	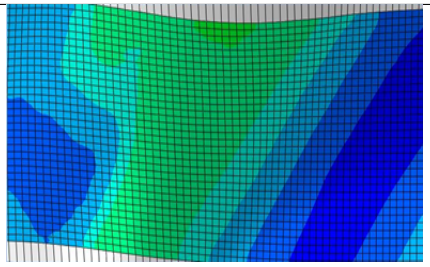
Bilinear	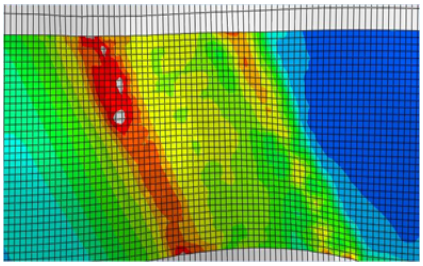	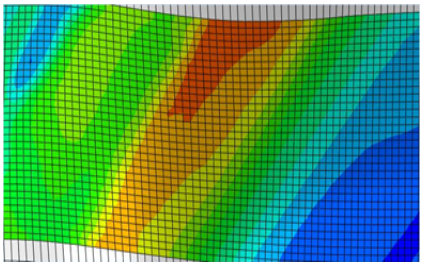
Multilinear	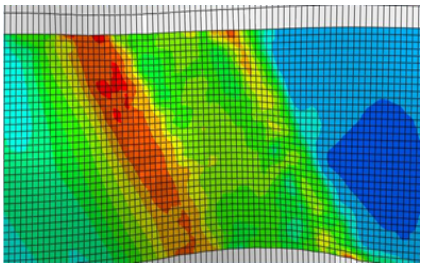	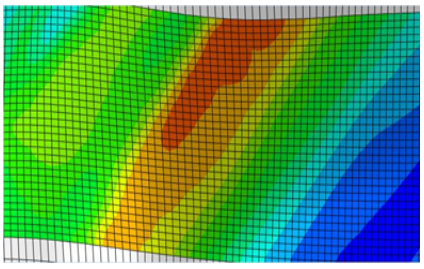
Johnson-Cook	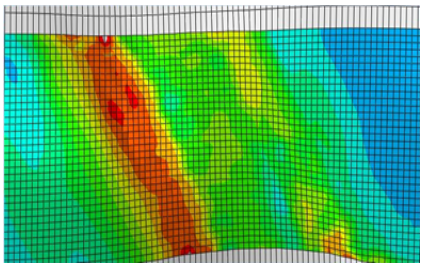	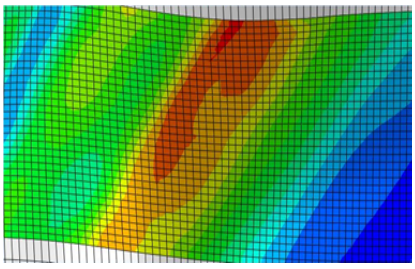

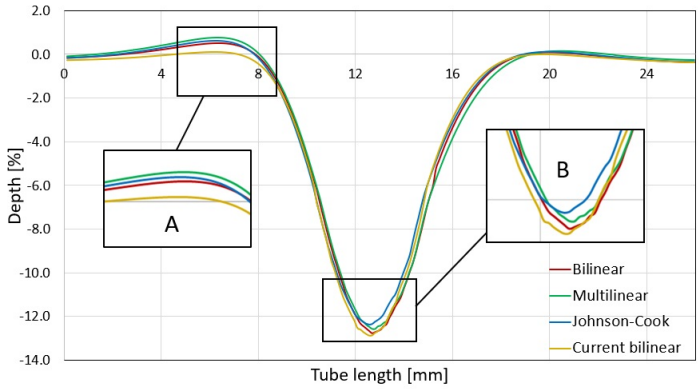

(a) Outer profile

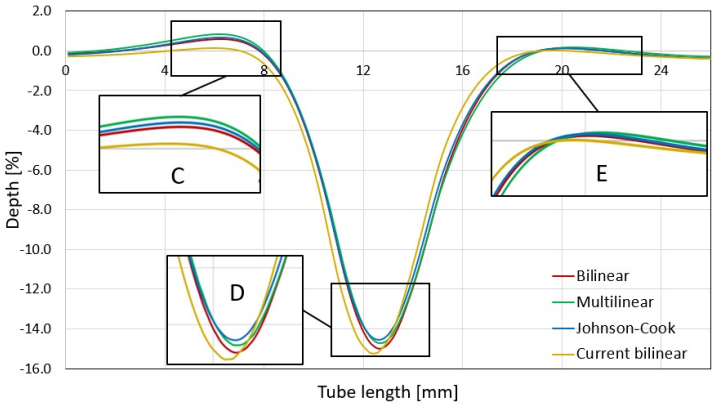

(b) Inner profile

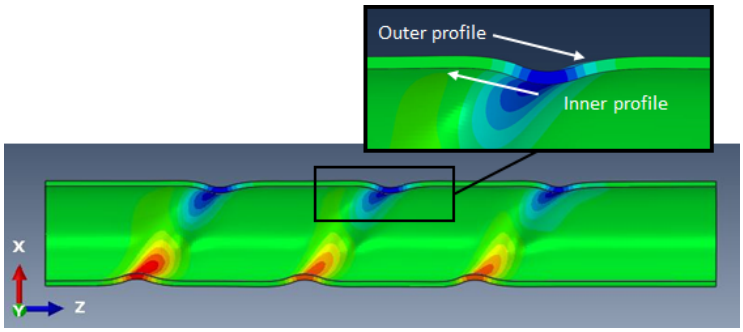

Figure 5.14: Comparison of the outer and inner profile for the different material model.

5.2 Discussion

Tensile test

From the test machine, the outputs were the force, extension and engineering strain from the video extensometer. The engineering strain cannot be calculated using the measured extension from the machine, since it includes the interactions of the grips to the specimen. Instead, the true stress-strain curve is obtained using Eq. (3.5) and Eq. (3.8) with the engineering strain, ε, measured from the video extensometer for more accurate results.

In Fig. 5.1, three samples and the average of the test with the same conditions is observed. As it can be seen, the experimental curves are consistent. The elastic region is very small in comparison with the plastic region as expected. The material breaks when the strain is around 43%, making 316L very ductile. At this strain, the corresponding ultimate tensile strength is roughly 990 MPa.

Fig. 5.2 compares the experimental stress-strain curves performed at different strain rates. It can be hard to see the impact from the different strain rates. For the sake of clarity, the differences are listed in Table 5.1, where a significant increase in yield stress is noted. This means the mechanical behaviour of the material is strain-rate-dependent. To further investigate the effect of strain-rate, the variation of the stress are plotted with respect to the logarithmic strain-rate as seen in Fig. 5.3. It is done for four levels of strain: at yielding, 5%, 15% and 25%. The highest increase in stress with increasing strain rate is at yielding and this is the impact of strain rates that is expected for the material. If the variation of tested strain rates was wider as in article [9], the impact would be clearer.

When looking at the Young's modulus of the performed tensile tests, some differences can be observed in Table 5.1. It may be due to the inability of the video extensometer to track the gauge points at different strain rates accurately, especially in a small region

as elastic one. Therefore, one test was performed with a bigger specimen to capture a more consistent deformation in the elastic region. Another possible reason that can affect this material property is how the specimen is loaded into the machine. In order to obtain an accurate value of the Young's modulus, the specimen must be placed parallel to the direction of the applied load. It must be noted that the Young's modulus is a material property in the elastic region and does not depend on the specimen geometry nor on the strain rate.

Virtual tensile test

Results from the bilinear material model under quasi-static loading condition are plotted in Fig. 5.4 with a comparison to the experimental curves. A good agreement can be observed in the elastic region. A significant difference between the results from using the material model and experimental data, can be noted beyond the yielding. It is seen from the figure that the onset of plastic deformation occurs at a lower value of strain. An underprediction of the stresses can be seen up to a strain of about 35%. While at larger plastic strains, the stresses are overestimated.

In order to get a more accurate result in the plastic region, a multilinear model was used. Looking at the results from the multilinear model, shown in Fig. 5.5, it can be seen that the model agrees with the experimental curve both in the elastic and plastic region. The more stress-strain points that are chosen, the more accurate is the curve fitting with this material model. Just as for the bilinear material model, the curve fittings are only valid for this quasi-static case. For other strain rates, new predictions need to be made or take use of a rate-dependent model, e.g. Cowper-Symonds (see Section 2.5.1).

Implementing the Johnson-Cook material model, the results obtained from the virtual quasi-static tensile test are seen in Fig. 5.6. A comparison on how well this model fits the experimental can be made. From observation, the numerical values seem to capture

both the elastic and plastic response. The curve fitting is valid for strain rates that are considered quasi-static. For higher strain rates, the rate-dependent relation parameters need to be included as explained in Section 2.5.2.

Table 5.2 tells how well the material models fit the experimental data. All three models have an R^2-value that is above 0.99, indicating that the fit of the models are more than 99% accurate. Thus, the material model that has the highest R^2-value, gives the best fit to the experimental result. With that in mind, it is noted that the multilinear model gives the best fit, which is due to the multiple points that are used to describe the material behaviour in the plastic region.

It is important to note that the bilinear and multilinear models have an upper stress-strain limit. After this limit is exceeded, the solver assigns ideal plasticity behaviour. Therefore the models are only valid up until that point. The Johnson-Cook model does not have this behaviour since it is described with a set of parameters that relate the stress to any strain values. In Fig. 5.4-5.7, the stress-strain curves obtained from simulation are extrapolated for higher strains using a stress-strain relation for each model.

Fig. 5.7 compares the predictions of the proposed material models and the experimental curves under quasi-static loading condition. Once the equivalent stress value in Eq. (2.11) reaches the yield surface, the material begins to deform plastically. As it can be seen in the figure, all proposed material models predicted the onset of plasticity accurately. It can also be noted that the elastic region in all models are identical, while the major difference appears beyond the yielding. The proposed models are stiffer than the current model, which means a higher force is required to deform the material. It should also be noted that the current bilinear model has a lower fracture point (at 605MPa).

At the first time step, which corresponds to 0.1 mm displacement, distribution of the equivalent plastic strain and the von Mises effective stress are shown in Fig. 5.8 and Fig.

5.9 respectively, for the different material models. As seen in Fig. 5.8, the onset of plasticity occurs in the same region (seen as red marks) for all material models. The difference is how intense the plastic strain and the effective stress distribution are in the middle of the specimen. The field results, according to the Johnson-Cook model show that the specimen is less deformed. Especially in comparison with the current bilinear model which is easily deformed, i.e. softer. From Fig. 5.7, one can see how the different material models relate to one another when it comes to the onset of plasticity. The differences in plastic stress is confirmed when looking at the stress distribution in Fig. 5.9. The Johnson-Cook model can therefore be considered as stiffer than the other material models at this step.

The model response at 10 mm displacement is also shown for the different material models in Fig. 5.10 and Fig. 5.11. Significant deformation is already seen for the current bilinear model even though the stress is roughly half of what the material can withstand. The other three models, predict similar stress distribution. When it comes to PEEQ, the concentration is higher for the current bilinear material model. When looking at the stress distribution in Fig. 5.11, the material model that stands out is the current bilinear model. The stress level for this model is roughly half in comparison with the other models. However, the other material models show almost the same response.

Manufacturing process

Fig. 5.12 shows how the deformed tube looks like from the outside and the inside. A small section of the middle region is chosen for analysis with a fine mesh. Lines between the colored and grey element band are the transition lines of a fine to a coarse mesh. Therefore, results close to these transition lines are not accurate.

The plastic deformation in the deformation process occurs in a range of 20% to 35% according to the figures in Table 5.3. When deforming the tube using the current bilinear model, the maximum strain and stress value are beyond the fracture point (see Table 5.3). Use of this model in the deformation process will therefore result in failure of the material.

Comparing the proposed material models, the stress distribution according to Table 5.4 shows that the outer region of the tube is exposed to higher stress when using the bilinear model. The response using the multilinear and Johnson-Cook is similar. This is explained by Fig. 5.7, where one can see that the difference in stress values is small for these two models.

Effective strain rate results using the Johnson-Cook rate-dependent model are shown in Fig. 5.13. The results show that the deformation process is rate-dependent. Therefore, it is necessary to use a rate-dependent model.

The deformed profile for each material model are plotted in Fig. 5.14. When forming the profile, the deforming tool pushes the surface of the tube radially. Since the proposed models are stiffer than the current model, higher force is needed to deform the tube which results in bending of the tube. Therefore, the tube surface does not lie on the reference line, which can be seen in area A, C and E in Fig. 5.14. Use of the proposed material models results in uneven surface (see area A and C in Fig. 5.14).

6 Conclusions

The general purpose of this paper was to characterize the appropriate material model in material grade 316L to be used in FEA. For this purpose, samples of the material were tensile tested at three different strain rates and the plastic deformation was studied. The material behaviour was assumed independent of direction, i.e. isotropic.

To simulate the tensile test virtually, an FE model was created in HyperMesh with the same geomerty as the specimens. The material behaviour in the FE model was described using a current bilinear model and three proposed material models. These were, bilinear, multilinear and Johnson-Cook isotropic hardening models. The model parameters were calibrated from the quasi-static tests. A single element test was used to verify the material response before running the FE analyses.

Rate dependency of the material was also investigated using Cowper-Symonds and Johnson-Cook rate-dependent models. The rate-dependent parameters were determined using the dynamic tensile tests.

Comparisons of simulated response and experimental results were then made for verification of the material models. After the verification, the deformation process was simulated using these material models.

The following conclusions can be drawn from the work:

- The video extensometer was unable to capture accurate displacements of the gauge points in the elastic region. Therefore, a mechanical extensometer was used.
- In the physical tensile test, 316L was deformed up to 43% strain, proving that the material is ductile.
- The plastic deformation behaviour of 316L at different strain-rates showed to be rate-dependent. Increase of the strain rate resulted in increase of the yield stress.
- Results from the virtual tensile tests under quasi-static loading condition showed; the current bilinear model underpredicted the stress that the material can withstand. The multilinear and Johnson-Cook models gave a better prediction compared to the bilinear model.
- To capture the rate dependency of 316L, the Cowper-Symonds and Johnson-Cook models were used. To obtain the C-S paramters, a wider range of strain rates were required. Johnson-Cook rate-dependent model provided a good prediction for different strain rates.
- Results from the manufacturing process showed that use of the current bilinear model results in the failure of the material. Johnson-Cook rate-dependent model showed that the deformation process is rate-dependent. Using the bilinear or multilinear model would not take the strain-rate dependency of the process into account.

6.1 Source of errors

As mentioned earlier, different sources of experiments will give other data values. This is expected due to the way the material is treated before and during testing. Moreover, simplifications and assumptions are made when analyzing the obtained data. These factors that can contribute to errors are listed below for this work:

- No study was made on how the waterjet affects the material properties.
- To get more accurate results, the specimen must be kept vertical and parallel to the direction of the applied load.
- The curve fitting in elastic region is made for a few data points to result in a Young's Modulus that lies in the range of what theory suggests.
- The higher the strain rates, the harder it is for the video extensometer to record accurate elongation of the specimen.
- The material is assumed to be isotropic for simplicity and to allow use of Johnson-Cook as it is one of the most used material models for 316L.
- The geometric imperfections - it is almost impossible to produce an ideal specimen.
- Most engineering materials are in-homogeneous - the in-homogeneity of the material was not taken into consideration in the FE model.

7 Future work

- It would be of interest to perform experiments with strain rates of around $300s^{-1}$ since the manufacturing process seem to perform at the same magnitude. A popular experimental technique for the study of materials at high strain rates is the Split Hopkinson Pressure Bar (SHPB). With this, one is able to induce strain rates with a magnitude of some thousand of s^{-1}. Other parameters that describe the rate effects would be established. Consequently, more accurate material models would be obtained when combining results from quasi-static and dynamic tests. [18]

- Many research work on 316L do not consider anisotropy of the material. Since the deformation of the tube is done in a certain angle, a suggestion would be to implement a material model that takes anisotropy into account at that angle.

- Performing DIC (Digital Image Correlation) analysis on the specimens would have provided a better understanding on the deformations. Consequently, comparisons with the virtual tensile test field results would have been made easier. Also, DIC used with a 3D camera can be used to give an accurate value of the Poisson's ratio.

Bibliography

[1] Ottosen, N.S. and Ristinmaa, M. (2005). *The mechanics of constitutive modeling.* Amsterdam: Elsevier Science.

[2] *Mendelson, A. (1968). Plasticity: Theory and Application.* New York: Krieger.

[3] Besson, J., Cailletaud, G., Chaboche, J.-L., Forest, S. and Blétry, M. (2010). *Non-linear Mechanics of Materials.* Dordrecht: Springer.

[4] Marciniak, Z., Duncan, J.L. and Hu, S.J. (2002). *Mechanics of Sheet Metal Forming.* Oxford: Butterworth-Heinemann.

[5] Krenk, S. (2009). *Non-linear Modeling and Analysis of Solids and Structures.* Cambridge, UK: Cambridge University Press.

[6] Wufengyun.com. (2019). *Abaqus 6.14 Documentation.* [Online]. Available at: http://wufengyun.com:888/ [Accessed 20 May 2019].

[7] Ray, R.G. (2015). *Elasto-plastic Analysis of Plate Using Abaqus.* Rourkela Odisha, India: National Institute of Technology, Department of Civil Engineering.

[8] Sobolev, A. and Radchenko, M. (2016). *Use of Johnson-Cook plasticity model for numerical simulations of the SNF shipping cash drop tests.* Nuclear Energy and Technology, 2(4), pp. 272-276.

[9] Peroni, L. et al. (2014). *Investigation of the mechanical behaviour of AISI 316L stainless steel syntactic foams at different strain-rates.* Composites Part B: Engineering, vol. 66, pp. 430-442.

[10] Karkalos, N. and Markopoulos, A. (2018). *Determination of Johnson-Cook material model parameters by an optimization approach using the fireworks algorithm.* Procedia Manufacturing, vol. 22, pp. 107-113.

[11] Kim, J., Kim, S., Lee, C., Kim, M. and Lee, J. (2014). *A constitutive equation for predicting the material non-linear behaviour of AISI 316L, 321, and 347 stainless steel under low-temperature conditions.* International Journal of Mechanical Sciences, vol. 87, pp. 218-225.

[12] Palengat, M., Chagnon, G., Favier, D., Louche, H., Linardon, C. and Plaideau, C. (2013). *Cold drawing of 316L stainless steel thin-walled tubes: experiments and finite element analysis.* International Journal of Mechanical Sciences, vol. 70, pp. 69-78.

[13] Umbrello, D., M'Saoubi, R. and Outeiro, J. (2007). *The influence of Johnson–Cook material constants on finite element simulation of machining of AISI 316L steel.* International Journal of Machine Tools and Manufacture, vol. 47, no. 3-4, pp. 462-470.

[14] Caeai.com. (2019). CAE Associates. *The Importance of Including Strain-Rate Effects in Explicit Dynamics Material Models.* [Online]. Available at: https://caeai.com/blog/importance-including-strain-rate-effects-explicit-dynamics-material-models. [Accessed 01 June 2019].

[15] Škrlec, A. and Klemenc, J. (2016). *Estimating the Strain-Rate-Dependent Parameters of the Cowper-Symonds and Johnson-Cook Material Models using Taguchi Arrays.* Strojniški vestnik - Journal of Mechanical Engineering, vol. 62, no. 4, pp. 220-230.

[16] Keller, C., and Herbrich, U. (2017). *Plastic Instability of Rate-Dependent Materials- A Theoretical Approach in Comparison to FE-Analyses.* Salzburg, Austria: 11^{th} European LS-DYNA Conference 2017.

[17] Schwer, L. *Optional Strain-Rate Forms for the Johnson Cook Constitutive Model and the Role of the Parameter Epsilon_ 0^1*. 6th European LS-DYNA Users' Conference 2007.

[18] Peroni, L. et al. (2007). *Experimental Analysis of Nano Engineering Materials Structures.* pp. 291-292, 2p. Turin, Italy: Dipartimento di Meccanica, Politecnico di Torino.

[19] Course syllabus: Finite Element Method. (2019). [Online]. Available at: https://kurser.lth.se/kursplaner/19_20%20eng/FHLF20.html. [Accessed: 20 May 2019].

[20] Colin Cameron, A., Windmeijer, F. (1997). *An R-squared measure of Goodness-of-fit for some common nonlinear regression models.* Journal of Econometrics, vol. 77, no.2, p. 329-342.